

## Supporting Information

### for Electronic versus Steric Effects of Pyridinophane Ligands in Pd(III) complexes

Fengzhi Tang,<sup>†,Δ</sup> Sungho V. Park,<sup>†,Δ</sup> Nigam P. Rath,<sup>‡</sup> and Liviu M. Mirica<sup>†,\*</sup>

<sup>†</sup>Department of Chemistry, Washington University, One Brookings Drive, St. Louis, Missouri 63130-4899

and <sup>‡</sup>Department of chemistry and Biochemistry, University of Missouri-St. Louis, One University  
Boulevard, St. Louis, Missouri 63121-4400.

<sup>Δ</sup> The Author contributed equally to this work

### Table of Contents

<b>I. General specifications</b>	S2
<b>II. Synthesis of <sup>Me</sup>N4<sup>OMe</sup> and related Pd complexes</b>	S3
Synthesis of <sup>Me</sup> N4 <sup>OMe</sup>	S3
Preparation of ( <sup>Me</sup> N4 <sup>OMe</sup> )Pd <sup>II</sup> Cl <sub>2</sub>	S10
Preparation of ( <sup>Me</sup> N4 <sup>OMe</sup> )Pd <sup>II</sup> MeCl	S12
Preparation of [( <sup>Me</sup> N4)Pd <sup>III</sup> Cl <sub>2</sub> ](ClO <sub>4</sub> )	S14
Preparation of [( <sup>Me</sup> N4 <sup>OMe</sup> )Pd <sup>III</sup> Cl <sub>2</sub> ]ClO <sub>4</sub>	S15
Preparation of [( <sup>Me</sup> N4 <sup>OMe</sup> )Pd <sup>III</sup> MeCl]ClO <sub>4</sub>	S15
<b>III. Cyclic voltammograms of Pd<sup>II</sup> Complexes</b>	S16
<b>IV. UV-vis spectra of Pd<sup>III</sup> complexes</b>	S20
<b>V. EPR spectra of Pd<sup>III</sup> complexes</b>	S23
<b>VI. ORTEP and space filling models of Pd<sup>III</sup> complexes</b>	S26
<b>VII. Computational Details</b>	S28
<b>VIII. X-ray structure characterization of [1<sup>+</sup>]ClO<sub>4</sub>, [2<sup>+</sup>]ClO<sub>4</sub>, and [4<sup>+</sup>]ClO<sub>4</sub></b>	S49
<b>IX. References</b>	S60

## I. General specifications

All operations were performed under a nitrogen atmosphere using standard Schlenk and glove box techniques if not indicated otherwise. All reagents for which the syntheses are not given were purchased from Fisher Scientific, Sigma-Aldrich, Acros, STREM, or Pressure Chemical and were used as received without further purification. Solvents were purified prior to use by passing through a column of activated alumina using an MBRAUN SPS.  $(\text{PhCN})\text{Pd}^{\text{II}}\text{Cl}_2$ ,<sup>1</sup>  $(\text{COD})\text{Pd}^{\text{II}}\text{Cl}_2$ ,<sup>2</sup> and  $(\text{COD})\text{Pd}^{\text{II}}\text{MeCl}$ <sup>2</sup> were prepared according to literature procedures. The synthesis and characterization of complexes  $(^{\text{Me}}\text{N}_4)\text{Pd}^{\text{II}}\text{MeCl}$  and  $[(^{\text{Me}}\text{N}_4)\text{Pd}^{\text{III}}\text{MeCl}]^+$  were reported previously.<sup>3</sup> NMR spectra were obtained on a Varian Mercury-300 spectrometer (300.121 MHz) or a Varian Unity Inova-600 spectrometer (599.746 MHz). Chemical shifts are reported in parts per million (ppm) with residual solvent resonance peaks as internal references.<sup>4</sup> Abbreviations for the multiplicity of NMR signals are singlet (s), doublet (d), triplet (t), quartet (q), septet (sep), multiplet (m), broad resonance (br). UV-vis spectra were recorded on a Varian Cary 50 Bio spectrophotometer and are reported as  $\lambda_{\text{max}}$ , nm ( $\epsilon$ ,  $\text{M}^{-1}\text{cm}^{-1}$ ). EPR spectra were recorded on a JEOL JES-FA X-band (9.2 GHz) EPR spectrometer in 3:1 PrCN:MeCN at 77 K or 293 K. Solution magnetic susceptibility measurements for  $\text{Pd}^{\text{III}}$  complexes were obtained at 293 K by the Evans method<sup>4</sup> using coaxial NMR tubes and MeCN as solvent, and the corresponding diamagnetic corrections were included.<sup>5</sup> ESI-MS experiments were performed using a linear quadrupole ion trap Fourier transform ion cyclotron resonance mass spectrometer (LTQ-FTMS, Thermo, San Jose, CA) or a Bruker Maxis Q-TOF mass spectrometer with an electrospray ionization source. ESI mass-spectrometry was provided by the Washington University Mass Spectrometry Resource. Elemental analyses were carried out by the Columbia Analytical Services Tucson Laboratory and Intertek Pharmaceutical Services.

## Electrochemical measurements

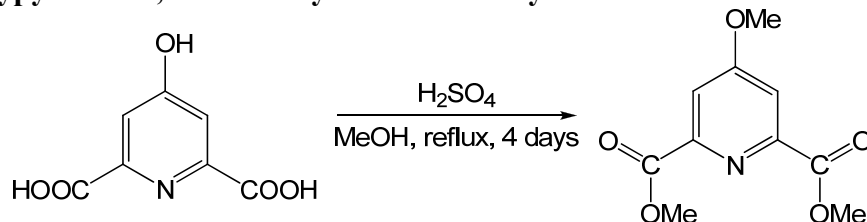
Cyclic voltammetry (CV) studies were performed with a BASi EC Epsilon electrochemical workstation or CHI Electrochemical Analyzer 660D. Electrochemical grade  $\text{Bu}_4\text{NClO}_4$  from Fluka were used as the supporting electrolytes. The electrochemical measurements were performed under a blanket of nitrogen, and the analyzed solutions were deaerated by purging with nitrogen. A glassy carbon disk electrode (GCE) was used as the working electrode, and a Pt wire as the auxiliary electrode. The non-aqueous Ag-wire reference electrode assembly was filled with 0.01 M  $\text{AgNO}_3/0.1$  M  $\text{Bu}_4\text{NClO}_4/\text{MeCN}$  solution. The reference electrodes were calibrated against ferrocene for each CV measurement.

Bulk electrolysis oxidations were performed in a two-compartment bulk electrolysis cell (BASi) separated by a fine-frit glass junction at room temperature. A reticulated vitreous carbon working electrode was used in the anodic compartment equipped with a magnetic stirring bar. A Pt gauze (25 mm x 10 mm) was used as the auxiliary electrode in the cathodic compartment. A non-aqueous Ag/0.01 M  $\text{AgNO}_3$  electrode was used as a reference electrode. Prior to electrolysis, a CV of the  $\text{Pd}^{\text{II}}$  precursor was performed in the same setup. The potential of electrolysis was set to be 100 mV-200 mV more positive than the corresponding oxidation peak potential observed in the CV scan. Electrochemical grade  $\text{Bu}_4\text{NClO}_4$  from Fluka was used as supporting electrolyte.

## II. Synthesis of <sup>Me</sup>N<sup>4</sup>OMe ligand and related Pd complexes

### Synthesis of <sup>Me</sup>N<sup>4</sup>OMe Ligand

#### 4-Methoxypyridine-2,6-dicarboxylic acid dimethyl ester<sup>6</sup>



Chelidamic acid monohydrate (1.31 g) was refluxed in ~300 mL dry methanol in the presence of 6 mL concentrated sulfuric acid for 4 days. After cooling down to RT, sodium carbonate (1 equiv relative to the amount of sulfuric acid) was added and the solvent was removed. The residue was dissolved in saturated aqueous sodium bicarbonate solution and then extracted with dichloromethane (DCM). The organic layer was dried over sodium sulfate and filtered, the solvent was removed and the white solid was dried *in vacuo*. Yield: 0.81 g (55%).

$^1\text{H}$  NMR (300MHz,  $\text{CDCl}_3$ ),  $\delta$ : 7.82 (s, 2H, arom-H), 4.01 (s, 6H,  $-\text{COOCH}_3$ ), 3.98 (s, 3H, *p*- $\text{OCH}_3$ ).

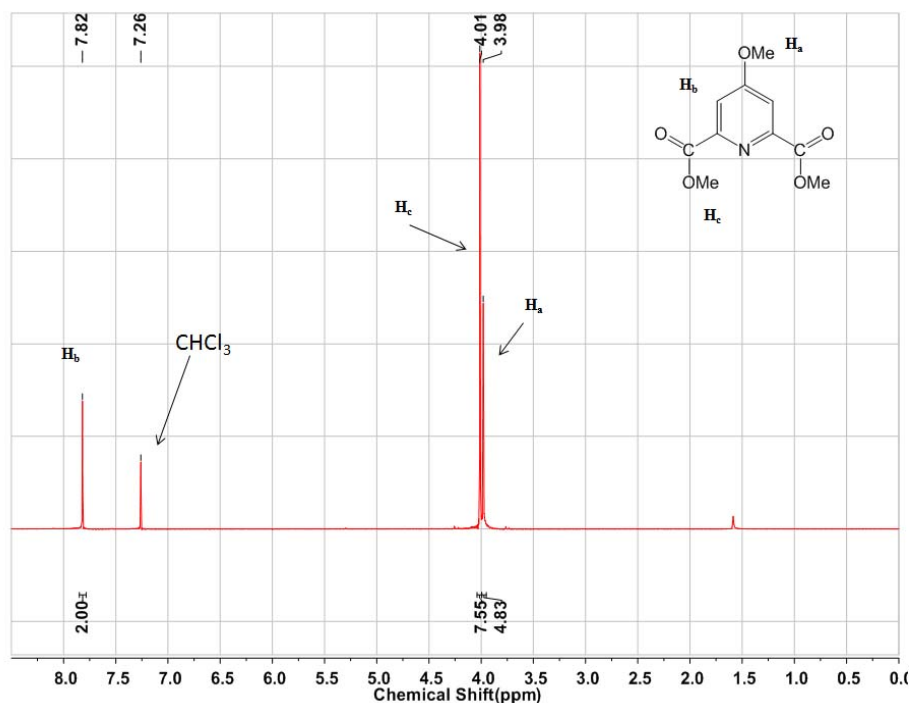
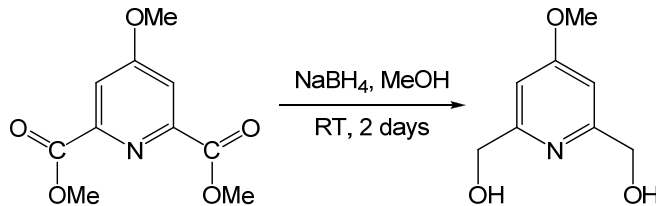


**Figure S1.**  $^1\text{H}$  NMR spectrum of 4-methoxypyridine-2,6-dicarboxylic acid dimethyl ester in  $\text{CDCl}_3$ .

## 4-Methoxy-2,6-bis(hydroxymethyl)pyridine



To 2.22 g of 4-methoxypyridine-2,6-dicarboxylic acid dimethyl ester in 50 mL methanol, sodium borohydride (5 equiv, 1.86 g) was slowly added. As the mixture refluxed, the color changed from colorless to yellow, and then to white. The resulting solution was stirred at room temperature for 2 days. The solvent was then removed under reduced pressure and the residue was dissolved in 30 mL of saturated NaHCO<sub>3</sub> solution. The solution was extracted with DCM, and the organic and aqueous layers were dried separately. The aqueous layer residue was extracted with 100 mL chloroform using a Soxhlet extractor for 2 days at 80 °C. Yield: 0.90 g (54 %).

<sup>1</sup>H NMR of 4-Methoxy-2,6-bis(hydroxymethyl)pyridine (300MHz, CDCl<sub>3</sub>), δ: 6.71 (s, 2H, arom-H), 4.71 (s, 4H, -CH<sub>2</sub>-), 3.86 (s, 3H, *p*-OCH<sub>3</sub>).

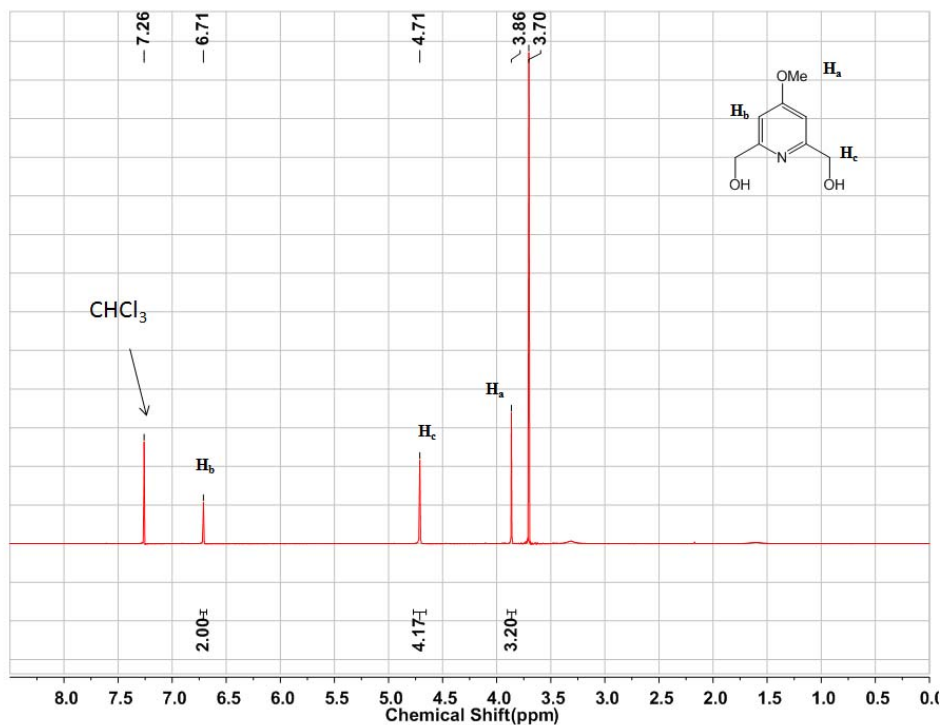
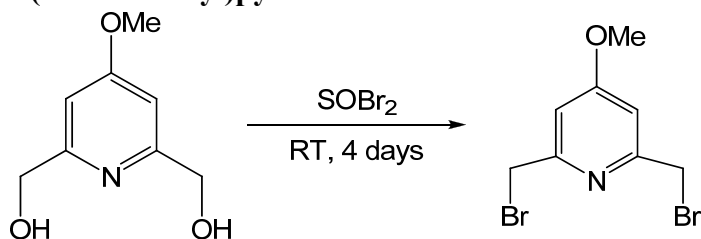


Figure S2. <sup>1</sup>H NMR spectrum of 4-Methoxy-2,6-bis(hydroxymethyl)pyridine in CDCl<sub>3</sub>.

#### 4-Methoxy-2,6-bis(bromomethyl)pyridine



4-methoxy-2,6-bis(hydroxymethyl)pyridine (2.97 g) was suspended in 125 mL dry DCM. A mixture of thionyl bromide (5 mL, 3.5 equiv) in 35 mL DCM was added dropwise at 0 °C. The mixture was stirred for 4 days in the dark, and then it was poured into 100 mL of ice-cold water. The aqueous layer was neutralized to pH 8 with 3M NaOH on an ice bath. The organic layer was separated, washed with 100 mL 1 M NaOH and then with 100 mL water. The DCM layer was then dried over sodium sulfate, filtered and concentrated to dryness. Yield: 4.41 g (85 %).

<sup>1</sup>H NMR of 4-Methoxy-2,6-bis(bromomethyl)pyridine (300MHz, CDCl<sub>3</sub>), δ: 6.89 (s, 2H, arom-H), 4.48 (s, 4H, -CH<sub>2</sub>-), 3.88 (s, 3H, *p*-OCH<sub>3</sub>).

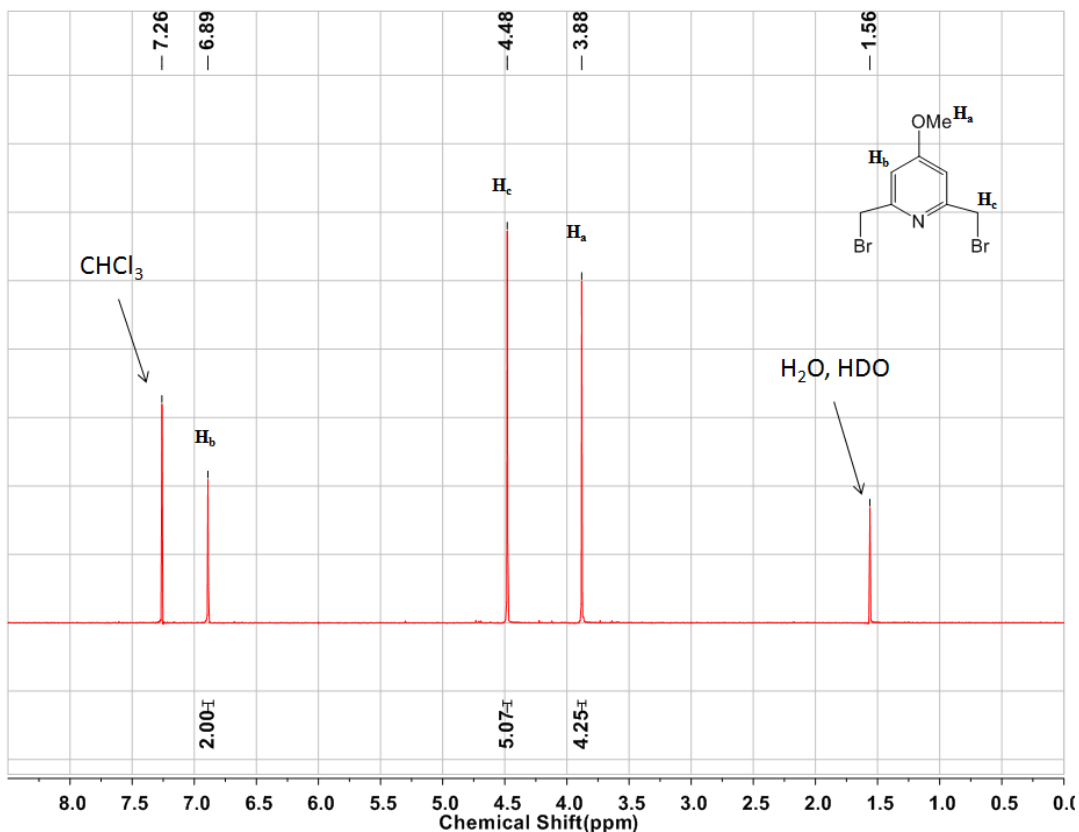
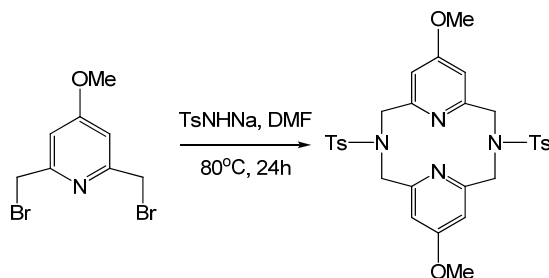


**Figure S3.** <sup>1</sup>H NMR spectrum of 4-Methoxy-2,6-bis(bromomethyl)pyridine in CDCl<sub>3</sub>.

## Methoxy *N,N'*-ditosyl-2,11-diaza[3.3](2,6)pyridinophane



4-methoxy-2,6-bis(bromomethyl)pyridine (4.41 g) in 40 mL anhydrous DMF was added dropwise to 2.884 g TsNHNa in 300 mL anhydrous DMF at 80°C. After the addition was complete, stirring was continued at 80°C for another hour. Another 2.884 g of TsNHNa was added all at once and heated at 80 °C overnight. After 24 h, the reaction mixture was cooled down to room temperature and the solvent was removed with reduced pressure. The brown residue was stirred with 150 mL MeOH for 10 minutes. The resulting suspension was filtered, washed with DI water and a small amount of methanol. The light yellow solid was dried *in vacuo*. Yield: 0.75g (33 %).

<sup>1</sup>H NMR of *p*-methoxy *N,N'*-ditosyl-2,11-diaza[3.3](2,6)pyridinophane (300 MHz, CDCl<sub>3</sub>), δ: 7.68 (d, *J* = 8 Hz, 4H, tosyl-arom-H), 7.35 (d, *J* = 8 Hz, 4H, tosyl-arom-H), 6.94 (s, 4H, pyr-arom-H), 4.92 (s, 8H, -CH<sub>2</sub>-), 4.00 (s, 6H, *p*-OCH<sub>3</sub>), 2.42 (s, 6H, tosyl-CH<sub>3</sub>).

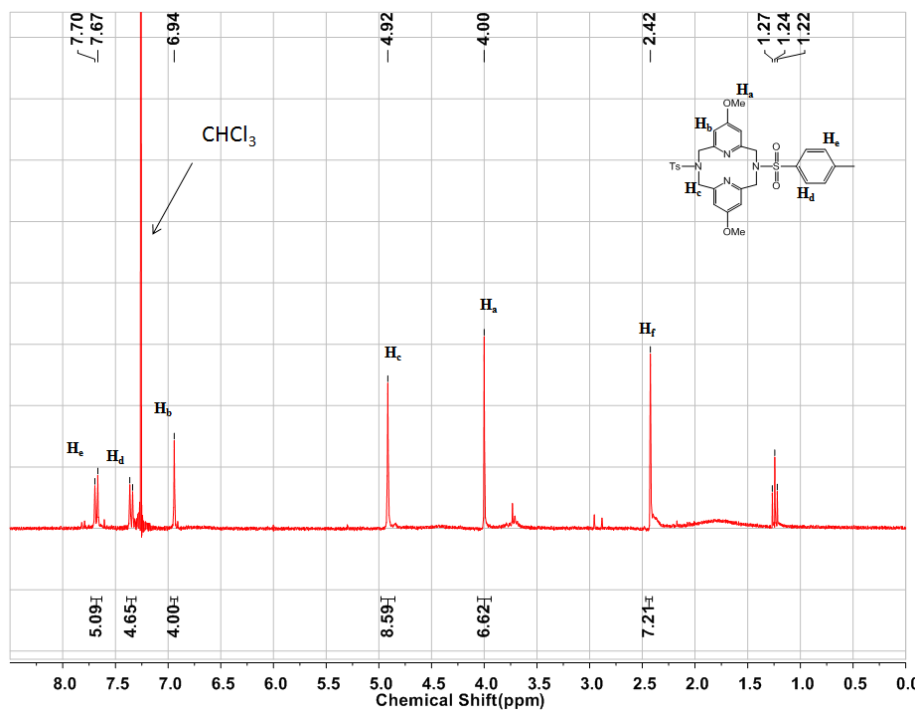
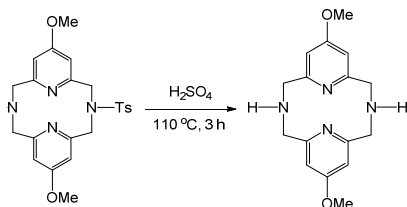


**Figure S4.** <sup>1</sup>H NMR spectrum of *p*-methoxy *N,N'*-ditosyl-2,11-diaza[3.3](2,6)pyridinophane in CDCl<sub>3</sub>.

## Methoxy 2,11-diaza[3.3](2,6)pyridinophane ( $\text{HN4OMe}$ )



To 1.75 g of *p*-methoxy *N,N'*-ditosyl-2,11-diaza[3.3](2,6)pyridinophane, 13.7 mL of 90 %  $\text{H}_2\text{SO}_4$  was added and the solution was stirred at 110 °C for 3 hours. After cooling down to room temperature, the solution was diluted with 65 mL water and treated with 3 M NaOH to adjust the pH to 12-13. The resulting solution was extracted with DCM 3 times, dried over  $\text{Na}_2\text{SO}_4$ , and dried under vacuum. Yield: 0.77 g (92 %).

$^1\text{H}$  NMR of *p*-methoxy 2,11-diaza[3.3](2,6)pyridinophane (300 MHz,  $\text{CDCl}_3$ ),  $\delta$ : 6.06 (s, 4H, arom-H), 3.86 (s, 8H,  $-\text{CH}_2-$ ), 3.66 (s, 6H, *p*- $\text{OCH}_3$ ).

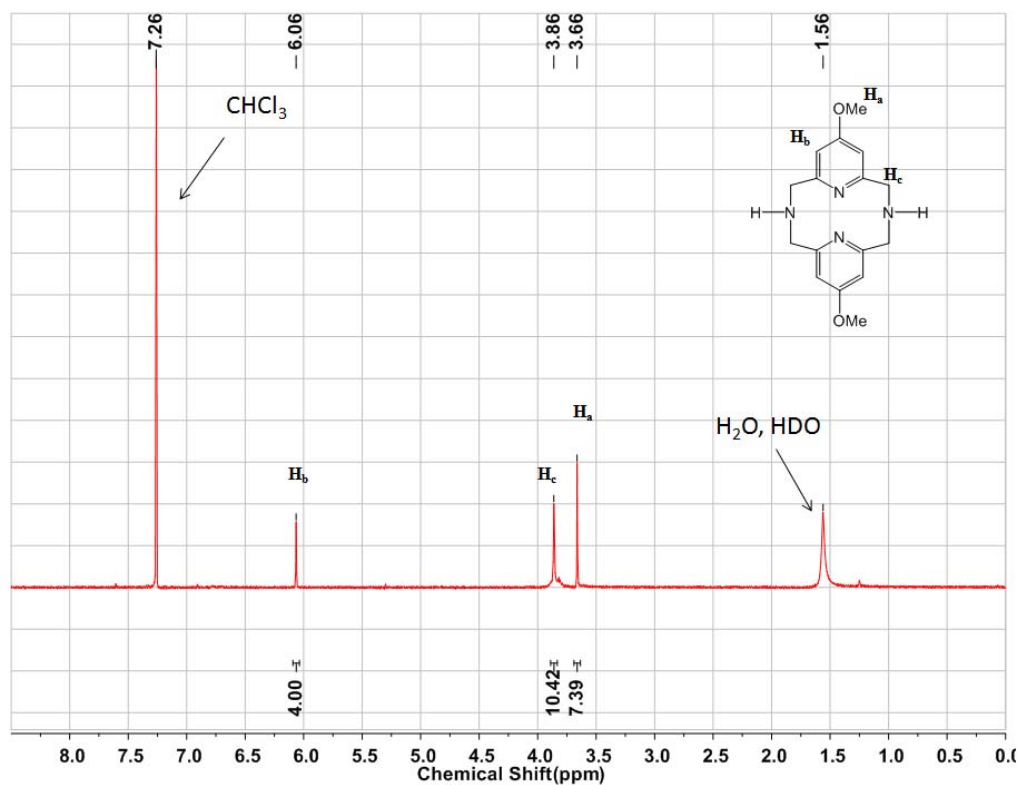
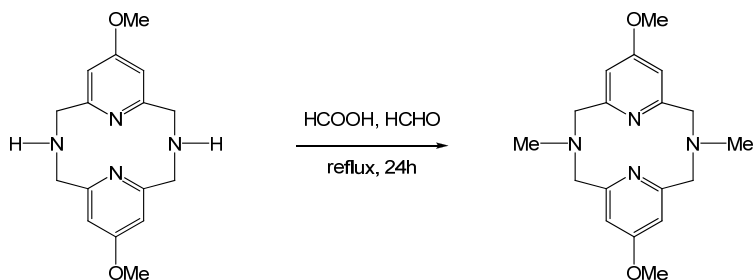


**Figure S5.**  $^1\text{H}$  NMR spectrum of *p*-methoxy 2,11-diaza[3.3](2,6)pyridinophane in  $\text{CDCl}_3$ .

**Methoxy *N,N'*-dimethyl-2,11-diaza[3.3](2,6)pyridinophane ( $\text{Me}_2\text{N}_4^{\text{OMe}}$ )**



An Eschweiler–Clarke methylation was conducted by dissolving 0.77 g of  $\text{H}_2\text{N}_4^{\text{OMe}}$  in 114 mL HCOOH and 25 mL 37%  $\text{CH}_2\text{O}$ . The mixture was refluxed under nitrogen for 1 day. After cooling, the reaction mixture was treated with 13.6 mL 37% HCl and the solvent was removed under reduced pressure. The residue was diluted with 10 mL  $\text{H}_2\text{O}$  and basified with 1 M NaOH to pH 13. The mixture was extracted with DCM 3 times, the organic layer was dried over  $\text{Na}_2\text{SO}_4$ , filtered, and dried under vacuum. The white product was further purified by extraction into hexane and removal of the solvent. Yield: 580 mg (58 %).

$^1\text{H}$  NMR of  $\text{Me}_2\text{N}_4^{\text{OMe}}$  (300MHz,  $\text{CD}_3\text{CN}$ ),  $\delta$ : 6.35 (s, 4H, arom-H), 3.64 (s, 8H,  $-\text{CH}_2-$ ), 3.63 (s, 6H,  $p\text{-OCH}_3$ ), 2.63 (s, 6H, N- $\text{CH}_3$ ).

$^{13}\text{C}$  NMR of  $\text{Me}_2\text{N}_4^{\text{OMe}}$  (300MHz,  $\text{CDCl}_3$ ),  $\delta$ : 165.39 (py- $\text{C}_{\text{ortho}}$ ), 159.04 (py- $\text{C}_{\text{meta}}$ ), 109.16 (py- $\text{C}_{\text{para}}$ ), 65.94 ( $-\text{CH}_2-$ ), 54.94 ( $p\text{-OCH}_3$ ), 49.06 (N-methyl-C).

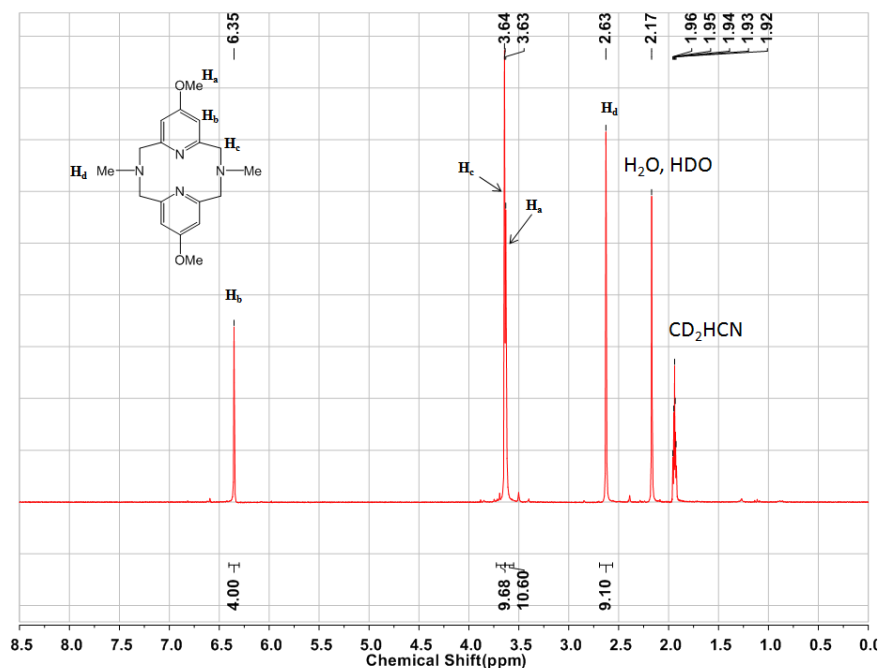


**Figure S6.**  $^1\text{H}$  NMR spectrum of  $\text{Me}_2\text{N}_4^{\text{OMe}}$  in  $\text{CD}_3\text{CN}$ .

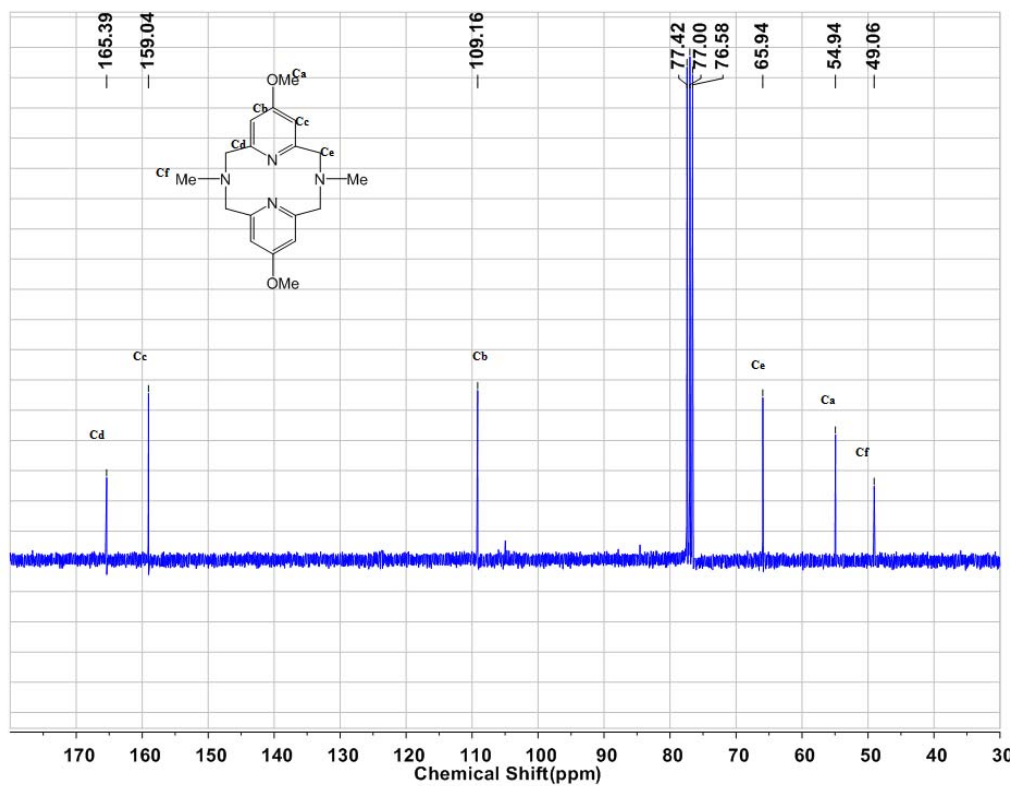
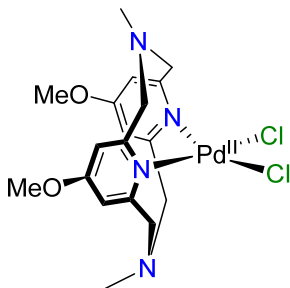


**Figure S7.**  $^{13}\text{C}$  NMR spectrum of  $\text{Me}_4\text{N}_4\text{OMe}$  in  $\text{CDCl}_3$ .

## Preparation of $(^{\text{Me}}\text{N}_4^{\text{OMe}})\text{Pd}^{\text{II}}\text{Cl}_2$ , 1



$^{\text{Me}}\text{N}_4^{\text{OMe}}$  (42.3 mg, 0.129 mmol) and  $(\text{PhCN})_2\text{Pd}^{\text{II}}\text{Cl}_2$  (49.4 mg, 0.129 mmol) were dissolved in 2 mL of dry DCM separately. The ligand solution was added dropwise to the precursor solution while the mixture was stirred. The solution turned brownish and cloudy, and stirring was continued for 24 hours. The gold yellow precipitate was filtered, washed with ether and pentane and dried *in vacuo*. Yield: 38.3 mg, 59 %.

*Alternative procedure.*  $^{\text{Me}}\text{N}_4^{\text{OMe}}$  (47.2 mg, 0.144 mmol) and  $(\text{COD})\text{Pd}^{\text{II}}\text{Cl}_2$  (41.0 mg, 0.144 mmol) were dissolved in 3 mL of DCM separately. The ligand solution was added dropwise to the precursor solution with stirring. After the addition was complete, the reaction mixture was stirred for an additional 24 hours in the dark. The clear, dark yellow solution eventually turned cloudy. The solvent was removed and the residue was dissolved in a minimum (2 mL) of DCM. This yellow mixture was filtered, washed with ether and pentane, and dried *in vacuo*. Yield: yellow powder, 62.9 mg, 86 %.

ESI-MS of  $(^{\text{Me}}\text{N}_4^{\text{OMe}})\text{Pd}^{\text{II}}\text{Cl}_2$  in MeCN,  $m/z$  469.0643; calculated for  $[\text{M}-\text{Cl}]^+$ ,  $\text{C}_{18}\text{H}_{24}\text{ClN}_4\text{O}_2\text{Pd}$ , 469.0643.

Anal. Found: C, 41.26; H, 4.46; N, 10.07; Calcd for  $(^{\text{Me}}\text{N}_4^{\text{OMe}})\text{Pd}^{\text{II}}\text{Cl}_2 \cdot \frac{1}{2}\text{CH}_2\text{Cl}_2$  ( $\text{C}_{18}\text{H}_{24}\text{Cl}_2\text{N}_4\text{O}_2\text{Pd}$ ) $\cdot\frac{1}{2}\text{CH}_2\text{Cl}_2$ : C, 40.53; H, 4.60; N, 10.22.

$^1\text{H}$  NMR (300 MHz,  $\text{CDCl}_3$ ): 6.65 (d,  $J = 15$  Hz, 4H,  $-\text{CH}_2-$ ), 6.61 (s, 4H, arom-H), 4.25 (d,  $J = 15$  Hz, 4H,  $-\text{CH}_2-$ ), 3.81 (s, 6H,  $p\text{-OCH}_3$ ), 2.33 (s, 6H, N- $\text{CH}_3$ ).

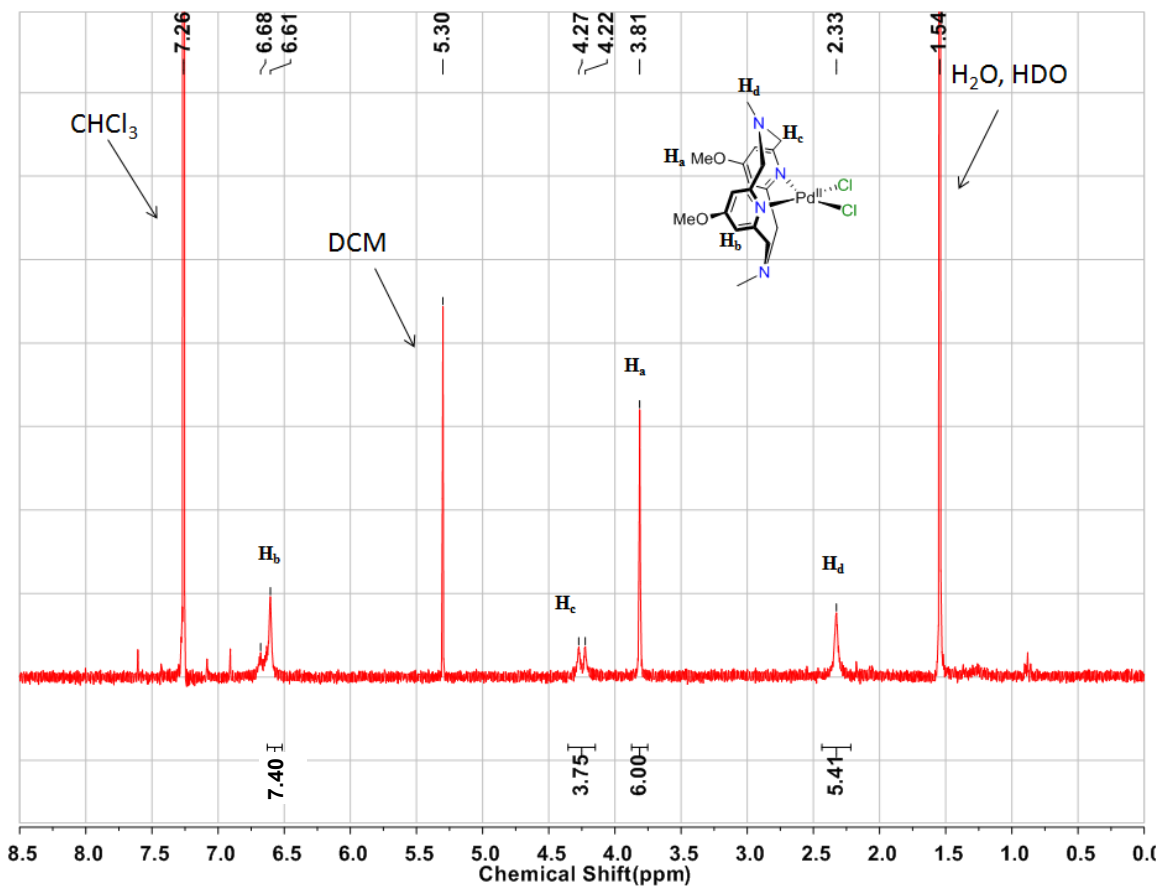
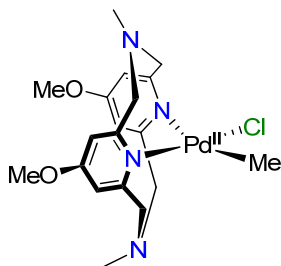


**Figure S8.**  $^1\text{H}$  NMR spectrum of  $(\text{Me}_4\text{N}_4\text{OMe})\text{Pd}^{\text{II}}\text{Cl}_2$  (**1**) in  $\text{CDCl}_3$ .

## Preparation of $(^{\text{Me}}\text{N}_4^{\text{OMe}})\text{Pd}^{\text{II}}\text{MeCl}$ , **4**



Under a nitrogen atmosphere,  $^{\text{Me}}\text{N}_4^{\text{OMe}}$  (44.3 mg, 0.135 mmol) and  $(\text{COD})\text{Pd}^{\text{II}}\text{MeCl}$  (35.5 mg, 0.135 mmol) were loaded in a round bottom flask. Anhydrous ethyl ether (15 mL) was added, and a light yellow suspension immediately formed. This suspension was stirred for 48 hours in the dark. The pale yellow precipitate was filtered, washed with ether and pentane and dried *in vacuo*. Yield: 45.5 mg, 70 %.

ESI-MS of solution of  $(^{\text{Me}}\text{N}_4^{\text{OMe}})\text{Pd}^{\text{II}}\text{MeCl}$  in MeCN,  $m/z$  449.1105; calculated for  $[\text{M}-\text{Cl}]^+$ ,  $\text{C}_{19}\text{H}_{27}\text{N}_4\text{O}_2\text{Pd}$ , 449.1169.

Anal. Found: C, 47.52; H, 5.66; N, 11.29; Calcd for  $(^{\text{Me}}\text{N}_4^{\text{OMe}})\text{Pd}^{\text{II}}\text{MeCl}$  ( $\text{C}_{19}\text{H}_{27}\text{ClN}_4\text{O}_2\text{Pd}$ ): C, 47.02; H, 5.61; N, 11.54.

$^1\text{H}$  NMR (300 MHz,  $\text{CDCl}_3$ ): 6.75 (s, 2H, arom-H), 6.75 (s, 2H, arom-H), 6.07 (d,  $J = 12$  Hz, 2H, -CH2-), 5.89 (d,  $J = 12$  Hz, 2H, -CH2-), 4.21 (d,  $J = 12$  Hz, 2H, -CH2-), 4.08 (d,  $J = 12$  Hz, 2H, -CH2-), 3.77 (s, 6H, p-OCH<sub>3</sub>), 2.31 (s, 6H, N-CH<sub>3</sub>), 0.41 (s, 3H, Pd-CH<sub>3</sub>).

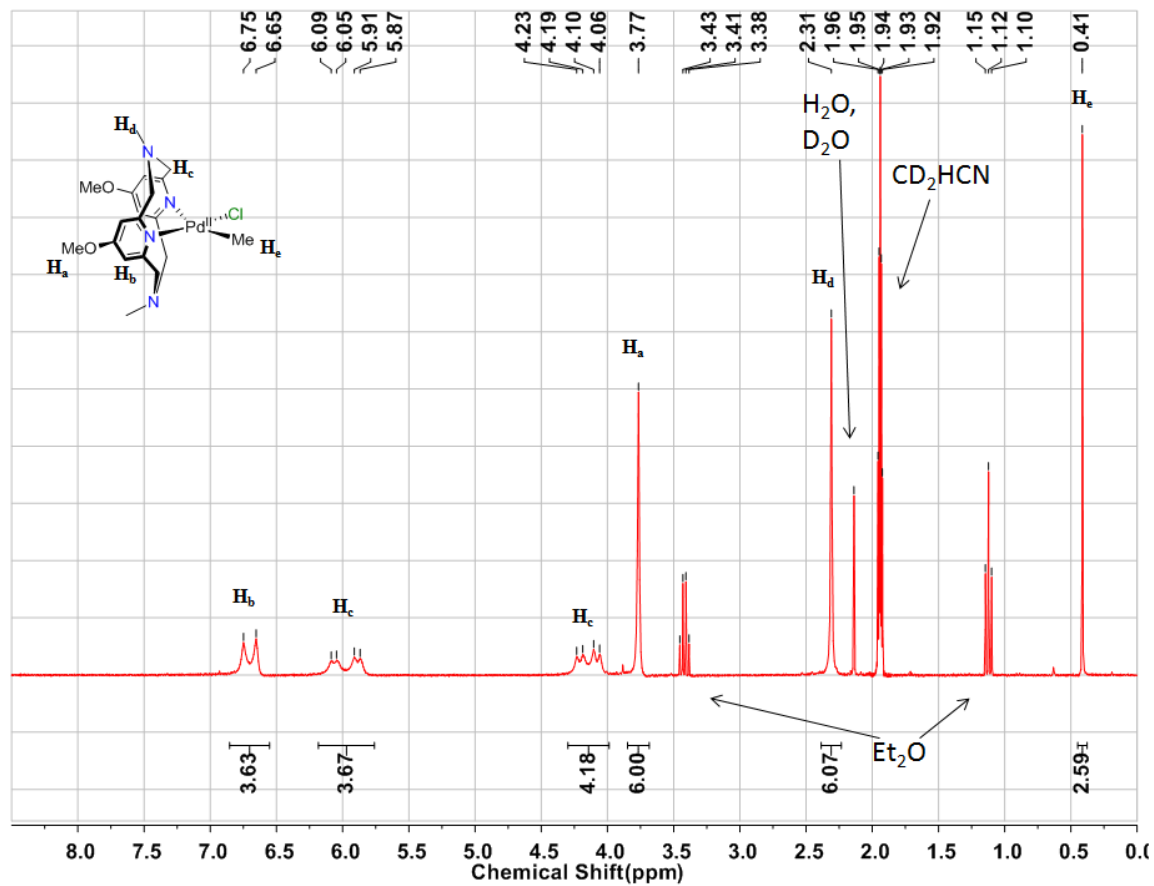
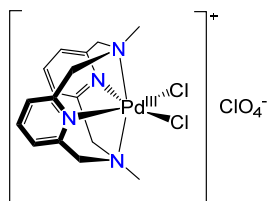


**Figure S9.**  $^1\text{H}$  NMR spectrum of  $(\text{Me}_4\text{N}_4\text{OMe})\text{Pd}^{\text{II}}\text{MeCl}$  (**4**) in  $\text{CDCl}_3$ .

## Preparation of $[(^{\text{Me}}\text{N}_4)\text{Pd}^{\text{III}}\text{Cl}_2](\text{ClO}_4)$ , $[2^+]\text{ClO}_4^-$



The controlled potential electrolysis of  $(^{\text{Me}}\text{N}_4)\text{Pd}^{\text{II}}\text{Cl}_2$  (74.1 mg, 0.166 mmol) was performed in 12 mL of 0.03 M  $\text{Bu}_4\text{NClO}_4/\text{MeCN}$  inside the working compartment of the electrolysis cell, while 12 mL 0.03 M  $\text{Bu}_4\text{NClO}_4/\text{MeCN}$  solution was inside the auxiliary compartment. The electrolysis potential was set as 470 mV *vs.*  $\text{Ag}/0.01\text{ M AgNO}_3$  based on the CV measured in the same electrolysis cell. The color of the solution turned dark purple quickly during the electrochemical oxidation process. The electrolysis was stopped when the electrolysis current decreased to a  $<5\ \mu\text{A}$ . The dark purple solution in the working compartment was filtered and the filtrate was set for ether diffusion at  $-20\ ^\circ\text{C}$ , to afford after a few days dark purple needle crystals suitable for X-ray crystallography. The crystals were filtered, washed with ether and pentane and dried *in vacuo*. Yield: 41.4 mg, 45 %.

UV-Vis,  $\lambda$ , nm ( $\epsilon$ ,  $\text{M}^{-1}\text{ cm}^{-1}$ ), MeCN: 578(1420), 362(2440)

$\mu_{\text{eff}} = 1.91\ \mu_{\text{B}}$  (Evans method,  $\text{CD}_3\text{CN}$ ).

ESI-MS of solution of  $[(^{\text{Me}}\text{N}_4)\text{Pd}^{\text{III}}\text{Cl}_2](\text{ClO}_4)$  in MeCN,  $m/z$  446.0107; calculated for  $[(^{\text{Me}}\text{N}_4)\text{Pd}^{\text{III}}\text{Cl}_2]^+$ ,  $\text{C}_{16}\text{H}_{20}\text{Cl}_2\text{N}_4\text{Pd}$ , 444.0100.

Anal. Found: C, 36.87; H, 4.14; N, 11.54; Calcd for  $[(^{\text{Me}}\text{N}_4)\text{Pd}^{\text{III}}\text{Cl}_2](\text{ClO}_4)\cdot\text{MeCN}$  ( $\text{C}_{18}\text{H}_{23}\text{Cl}_3\text{N}_4\text{O}_4\text{Pd}$ ): C, 36.88; H, 3.95; N, 11.95.

### Preparation of [(<sup>Me</sup>N<sub>4</sub><sup>OMe</sup>)Pd<sup>III</sup>Cl<sub>2</sub>]ClO<sub>4</sub>, [1<sup>+</sup>]ClO<sub>4</sub>

The controlled potential electrolysis of (<sup>Me</sup>N<sub>4</sub><sup>OMe</sup>)Pd<sup>II</sup>Cl<sub>2</sub> (74.1 mg, 0.166 mmol) was performed in 12 mL of 0.03 M Bu<sub>4</sub>NClO<sub>4</sub>/MeCN inside the working compartment of the electrolysis cell, while 12 mL 0.03 M Bu<sub>4</sub>NClO<sub>4</sub>/MeCN solution was inside the auxiliary compartment. The electrolysis potential was set as 260 mV vs. Ag/0.01 M AgNO<sub>3</sub> based on the CV measured in the same electrolysis cell. The color of the solution turned dark purple quickly during the electrochemical oxidation. The electrolysis was stopped after the charge corresponding to a one-electron oxidation has passed through the cell. The remaining dark purple solution was filtered and then diethyl ether was diffused at -20 °C for a few days to afford dark blue crystals suitable for X-ray crystallography. The crystals were filtered, washed with ether and pentane and dried *in vacuo*. Yield: 40 mg, 40 %.

UV-vis, λ, nm (ε, M<sup>-1</sup> cm<sup>-1</sup>), MeCN: 583 (960), 365 (2260), 325 (3060).

μ<sub>eff</sub> = 1.86 μ<sub>B</sub> (Evans method, CD<sub>3</sub>CN).

ESI-MS [(<sup>Me</sup>N<sub>4</sub><sup>OMe</sup>)Pd<sup>III</sup>Cl<sub>2</sub>]<sup>+</sup> in MeCN, m/z 484.0851; calcd. for [(<sup>Me</sup>N<sub>4</sub><sup>OMe</sup>)Pd<sup>III</sup>Cl<sub>2</sub>]<sup>+</sup>, 484.0857.

Anal. Found: C, 37.46; H, 4.43; N, 10.51; calcd. for [C<sub>18</sub>H<sub>24</sub>Cl<sub>3</sub>N<sub>4</sub>O<sub>6</sub>Pd•CH<sub>3</sub>CN]: C, 37.17; H, 4.21; N, 10.84.

### Preparation of [(<sup>Me</sup>N<sub>4</sub><sup>OMe</sup>)Pd<sup>III</sup>MeCl]ClO<sub>4</sub>, [4<sup>+</sup>]ClO<sub>4</sub>

Ferrocenium hexafluorophosphate (18.1 mg, 0.055 mmol) and (26.0 mg, 0.054 mmol) (<sup>Me</sup>N<sub>4</sub><sup>OMe</sup>)Pd<sup>II</sup>MeCl complex were combined in 5 mL MeCN and stirred for 30 minutes. The resulting solution was washed with pentane and concentrated with a rotary evaporator. The resulting dark purple residue was dissolved in a minimum of MeCN and divided into 3 batches. Concentrated solutions of ClO<sub>4</sub><sup>-</sup>, PF<sub>6</sub><sup>-</sup> and BF<sub>4</sub><sup>-</sup> were added to each batch and ether diffusion was conducted. Yield: 7.1 mg from BF<sub>4</sub><sup>-</sup> batch, 70 %; 6.3 mg from ClO<sub>4</sub><sup>-</sup> batch, 60 %. The characterization details below are for [(<sup>Me</sup>N<sub>4</sub><sup>OMe</sup>)Pd<sup>III</sup>MeCl]ClO<sub>4</sub>.

UV-vis, λ, nm (ε, M<sup>-1</sup> cm<sup>-1</sup>), MeCN: 615 (560), 495 (380), 303 (4700).

μ<sub>eff</sub> = 1.88 μ<sub>B</sub> (Evans method, CD<sub>3</sub>CN).

ESI-MS [(<sup>Me</sup>N<sub>4</sub><sup>OMe</sup>)Pd<sup>III</sup>MeCl]<sup>+</sup> in MeCN, m/z 504.0293; calcd. for [(<sup>Me</sup>N<sub>4</sub><sup>OMe</sup>)Pd<sup>III</sup>MeCl]<sup>+</sup>, 504.0311.

Anal. Found: C, 40.71; H, 4.82; N, 10.84; calcd. for [C<sub>19</sub>H<sub>27</sub>Cl<sub>2</sub>N<sub>4</sub>O<sub>6</sub>Pd•CH<sub>3</sub>CN]: C, 40.30; H, 4.83; N, 11.19.

### III. Cyclic voltammograms of Pd<sup>II</sup> Complexes

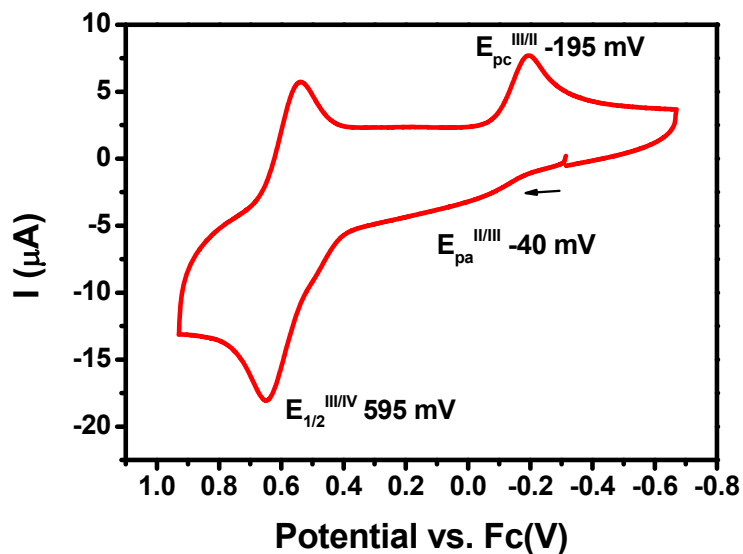


**Figure. S10.** Cyclic voltammogram (<sup>Me</sup>N4<sup>OMe</sup>)Pd<sup>II</sup>Cl<sub>2</sub> (**1**) in 0.1 M Bu<sub>4</sub>NClO<sub>4</sub>/DCM (GCE, 100 mV/s scan rate).

Potentials vs Fc/Fc<sup>+</sup> (mV):

$$E_{pa}^{II/III} = -40$$

$$E_{pc}^{III/II} = -195$$

$$E_{1/2}^{III/IV}(\Delta E_p) = 595 (110)$$

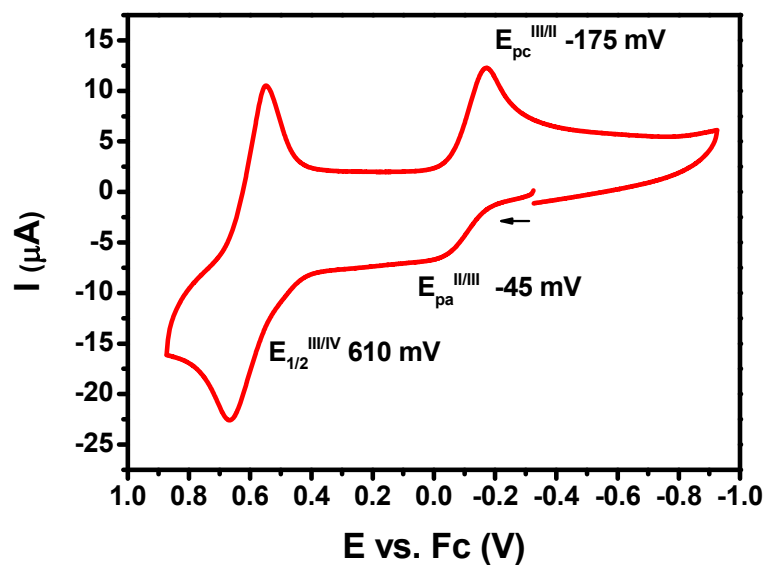


**Figure. S11.** Cyclic voltammogram ( $(\text{Me}_4\text{N})\text{Pd}^{\text{II}}\text{Cl}_2$  (**2**)) in 0.1 M  $\text{Bu}_4\text{NClO}_4/\text{DCM}$  (GCE, 100 mV/s scan rate).

Potentials vs  $\text{Fc}/\text{Fc}^+$  (mV):

$$E_{\text{pa}}^{\text{II/III}} = -45$$

$$E_{\text{pc}}^{\text{III/II}} = -175$$

$$E_{1/2}^{\text{III/IV}}(\Delta E_p) = 610 (115)$$

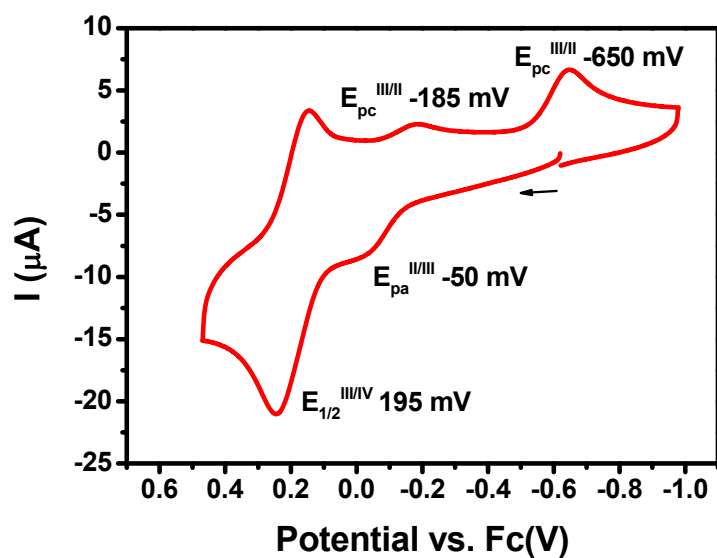


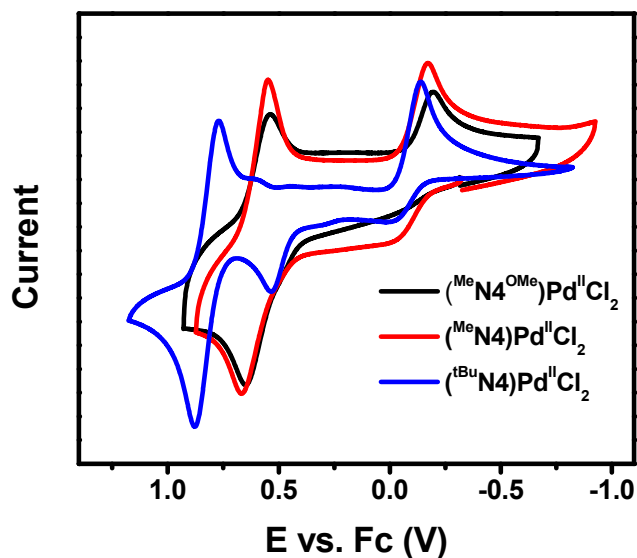
**Figure. S12.** Cyclic voltammogram ( $(\text{MeCN})_4\text{OMePd}^{\text{II}}\text{MeCl}$  (**4**)) in 0.1 M  $\text{Bu}_4\text{NClO}_4/\text{DCM}$  (GCE, 100 mV/s scan rate).

Potentials vs  $\text{Fc}/\text{Fc}^+$  (mV):

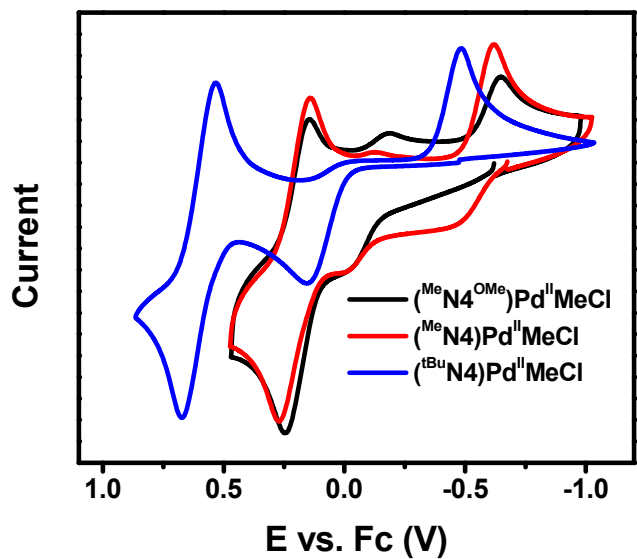
$$E_{\text{pa}}^{\text{III/II}} = -50$$

$$E_{\text{pc}}^{\text{III/II}} = -185, -650$$

$$E_{1/2}^{\text{III/IV}}(\Delta E_{\text{p}}) = 195 (100)$$

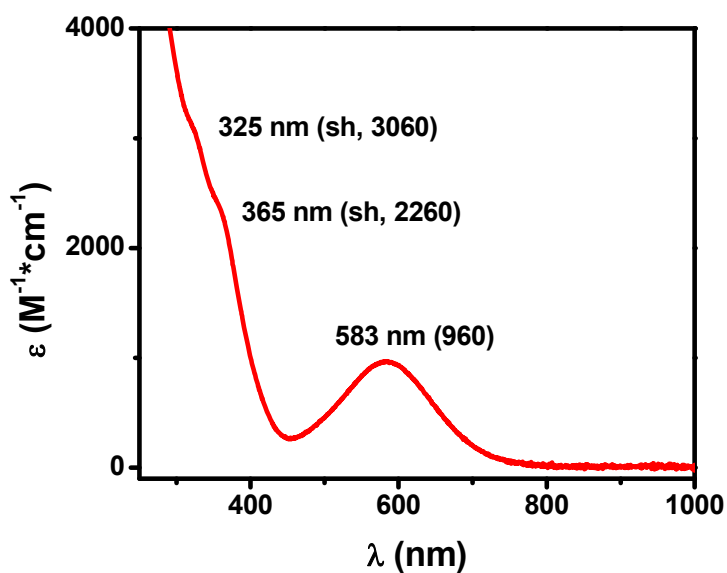


**Figure. S13.** Overlay of CVs of complexes 1-3 in 0.1 M Bu<sub>4</sub>NClO<sub>4</sub>/DCM (GCE, 100 mV/s scan rate).

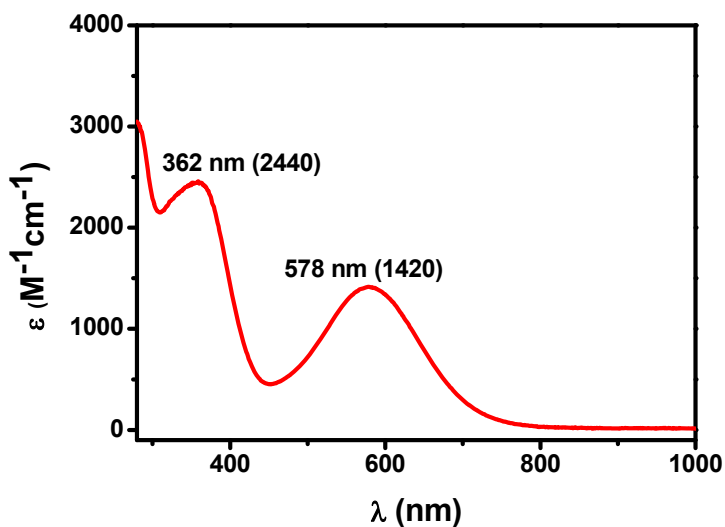


**Figure. S14.** Overlay of CVs of complexes 4-6 in 0.1 M Bu<sub>4</sub>NClO<sub>4</sub>/DCM (GCE, 100 mV/s scan rate).

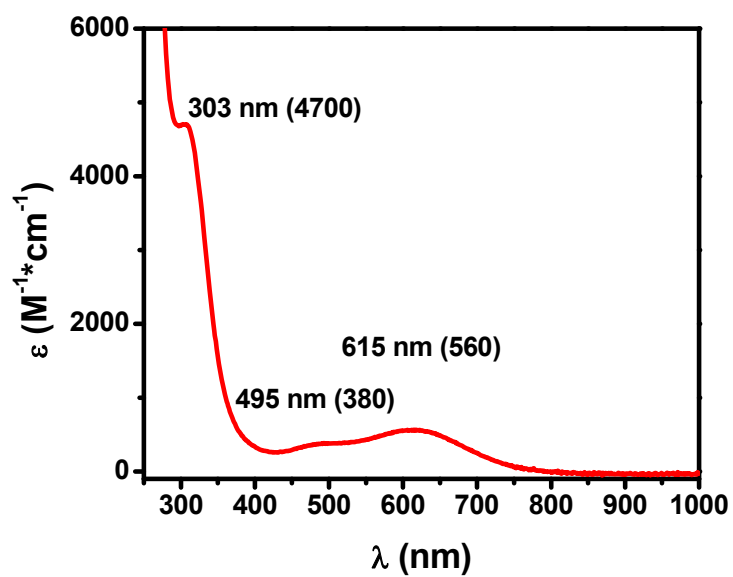
#### IV. UV-vis spectra of Pd<sup>III</sup> complexes



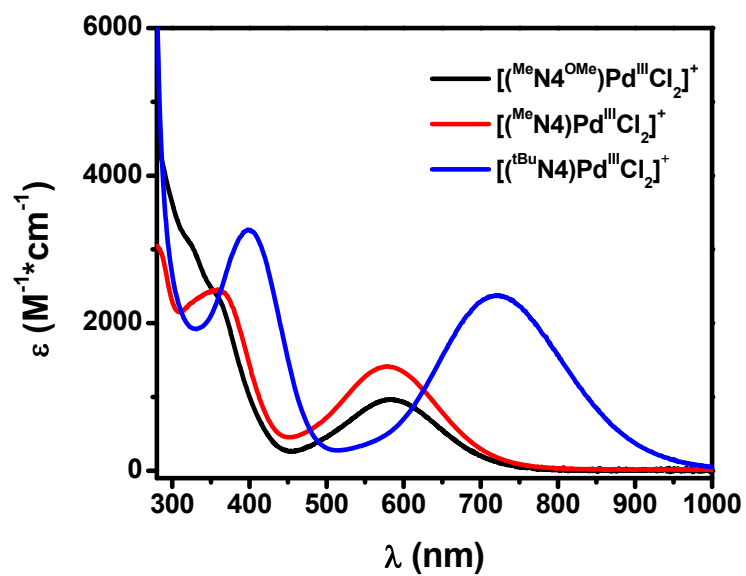
*Figure S15.* UV-vis spectrum of  $[(MeCN)_4Pd^{III}Cl_2]^+$  ( $1^+$ ) in MeCN.



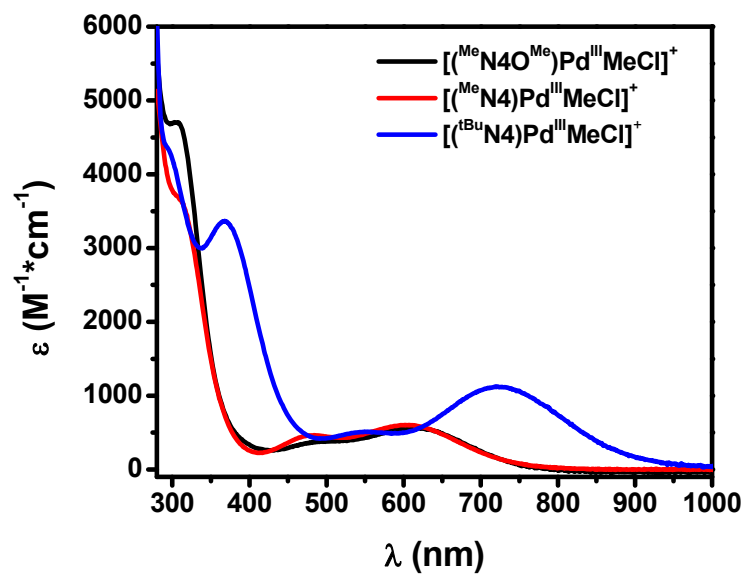
*Figure S16.* UV-vis spectrum of  $[(MeCN)_4Pd^{III}Cl_2]^+$  ( $2^+$ ) in MeCN.



**Figure S17.** UV-vis spectrum of  $[(^{\text{Me}}\text{N4}^{\text{OMe}})\text{Pd}^{\text{III}}\text{MeCl}]^+$  ( $4^+$ ) in MeCN.

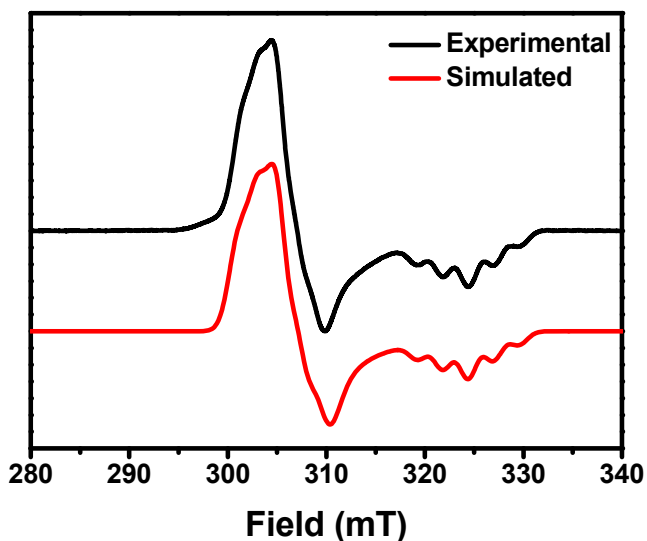


**Figure S18.** Overlay of UV-vis spectra of complexes  $1^+$ - $3^+$  in MeCN.

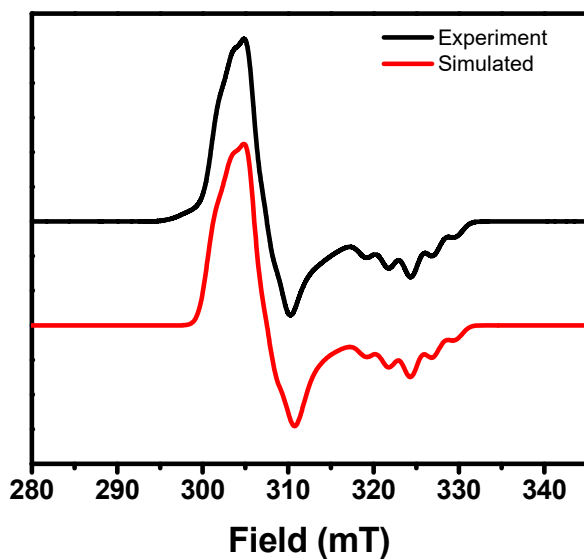


*Figure S19.* Overlay of UV-vis spectra of complexes 4<sup>+</sup>-6<sup>+</sup> in MeCN.

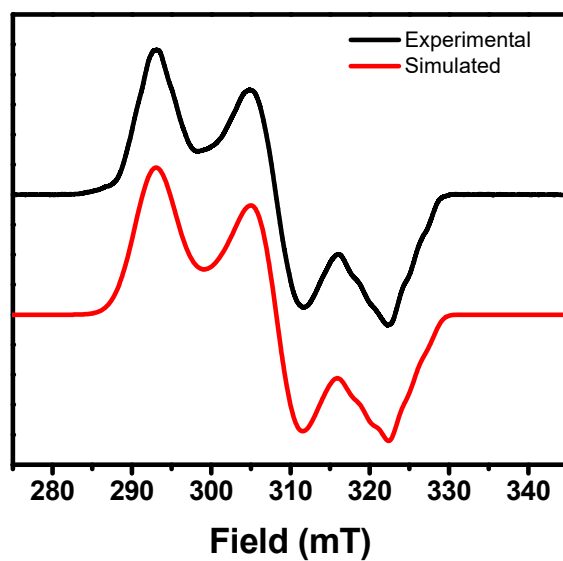
## V. EPR spectra of Pd<sup>III</sup> complexes



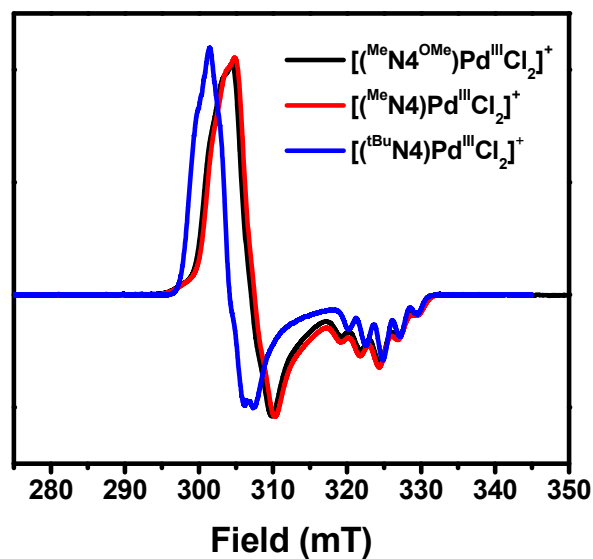
**Figure S20.** EPR spectrum of  $[(^{\text{Me}}\text{N}4^{\text{OMe}})\text{Pd}^{\text{III}}\text{Cl}_2]\text{ClO}_4$  ( $[1^+]\text{ClO}_4$ ) in 3:1 PrCN:MeCN glass, 77 K. Frequency: 9097.056 MHz. Simulated spectrum parameters:  $g_x = 2.129$  ( $A_N = 19.0$ , linewidth 20.0 G),  $g_y = 2.129$  ( $A_N = 19.0$ , linewidth 22.0 G),  $g_z = 2.0035$  ( $A_N = 25.5$  G, linewidth 17.5 G).



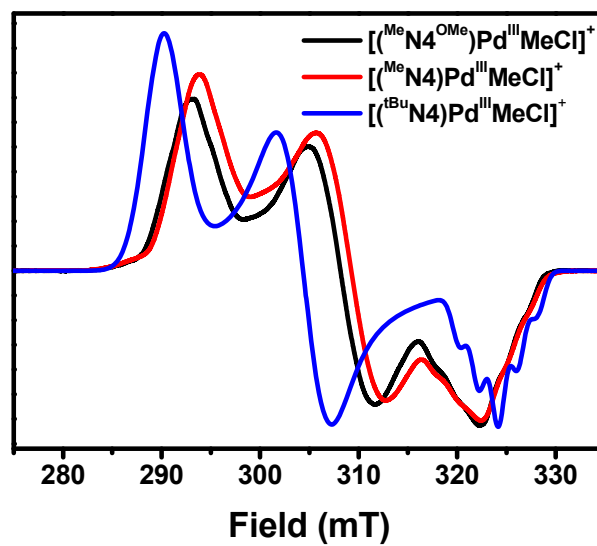
**Figure S21.** EPR spectrum of  $[(^{\text{Me}}\text{N}4)\text{Pd}^{\text{III}}\text{Cl}_2]\text{ClO}_4$  ( $[2^+]\text{ClO}_4$ ) in 3:1 PrCN:MeCN glass, 77 K. Frequency: 9095.776 MHz. Simulated spectrum parameters:  $g_x = 2.126$  ( $A_N = 19.0$ , linewidth 21.0 G),  $g_y = 2.126$  ( $A_N = 19.0$ , linewidth 21.0 G),  $g_z = 2.0035$  ( $A_N = 25.5$  G, linewidth 18.0 G).



**Figure S22.** EPR spectrum of  $[(^{\text{Me}}\text{N}4^{\text{OMe}})\text{Pd}^{\text{III}}\text{MeCl}]\text{ClO}_4$  ( $[\mathbf{4}^+]\text{ClO}_4$ ) in 3:1 PrCN:MeCN glass, 77 K. Frequency: 9096.719 MHz. Simulated spectrum parameters:  $g_x = 2.219$  ( $A_N = 0$ , linewidth 51.0 G),  $g_y = 2.108$  ( $A_N = 0$ , linewidth 51.0 G),  $g_z = 2.016$  ( $A_N = 23.0$  G, linewidth 22.0 G).

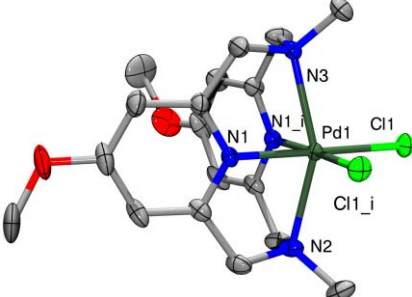
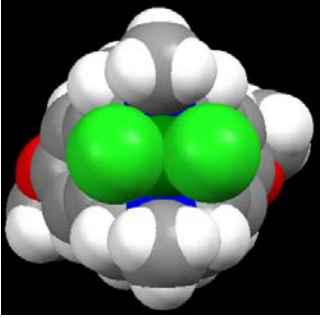
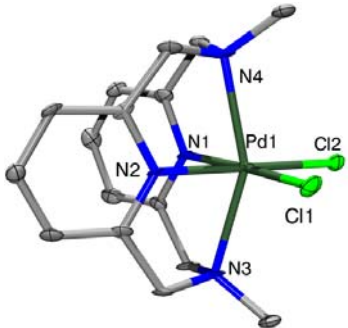
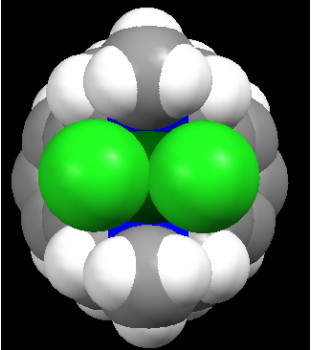
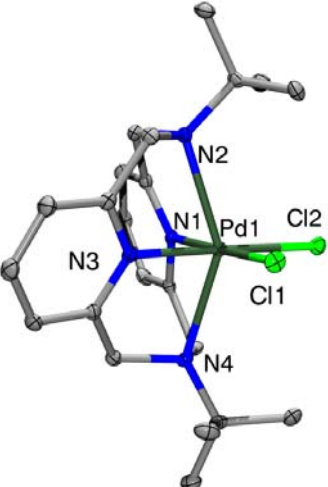
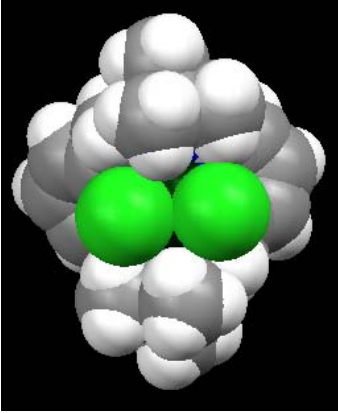


*Figure S23.* Overlay of EPR spectra of  $1^+$  -  $3^+$ .



*Figure S24.* Overlay of EPR spectra of  $4^+$  -  $6^+$ .

## VI. ORTEP and Space Filling Models of Pd<sup>III</sup> complexes

Side view of complexes	Selected bond distances and angles	Space filling model for the front view of complexes
<p><math>[(^{\text{Me}}\text{N4}^{\text{OMe}})\text{Pd}^{\text{III}}\text{Cl}_2]^+ (1^+)</math></p> 	<p>Pd1-N1 2.0009 (19) Å            Pd1-N1_i 2.0009(18) Å            Pd1-N2 2.300(3) Å            Pd1-N3 2.308(3) Å            Pd1-Cl1 2.3018(6) Å            Pd1-Cl1_i 2.3018(6) Å</p> <p>N1-Pd1-N1_i 82.67(11)            N2-Pd1-N3 152.89(10)°</p>	
<p><math>[(^{\text{Me}}\text{N4})\text{Pd}^{\text{III}}\text{Cl}_2]^+ (2^+)</math></p> 	<p>Pd1-N1 2.029(8) Å            Pd1-N2 2.002(8) Å            Pd1-N3 2.310(9) Å            Pd1-N4 2.311(9) Å            Pd1-Cl1 2.303(3) Å            Pd1-Cl2 2.322(3) Å</p> <p>N1-Pd1-N2 82.3(3)            N3-Pd1-N4 153.5(3)°</p>	
<p><math>[(^{\text{tBu}}\text{N4})\text{Pd}^{\text{III}}\text{Cl}_2]^+ (3^+)</math></p> 	<p>Pd1-N1 2.007(2) Å            Pd1-N3 1.999(2) Å            Pd1-N2 2.398(2) Å            Pd1-N4 2.436(2) Å            Pd1-Cl1 2.3119(7) Å            Pd1-Cl2 2.3201(7) Å</p> <p>N1-Pd1-N3 88.06(9)            N2-Pd1-N4 145.07(7)°</p>	

**Figure S25.** ORTEP diagrams and space filling models of  $[(^{\text{R}}\text{N4})\text{Pd}^{\text{III}}\text{MeCl}]^+$  complexes.

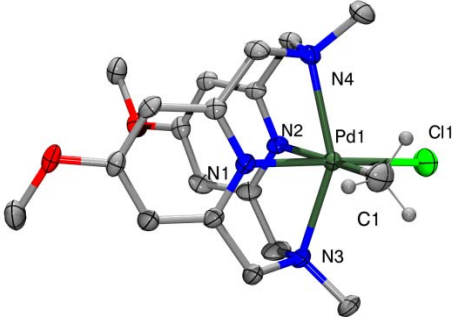
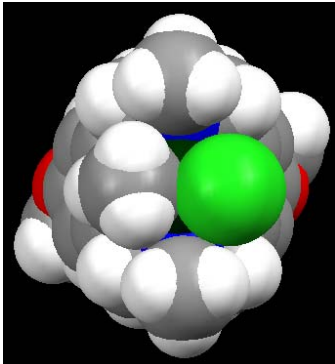
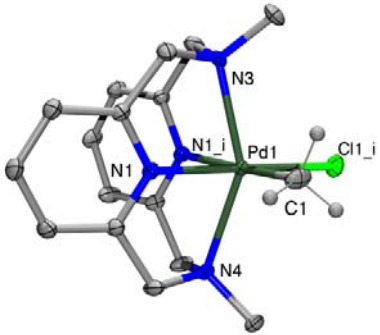
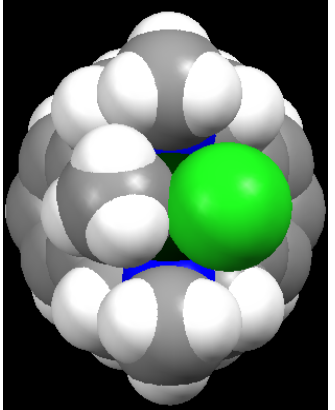
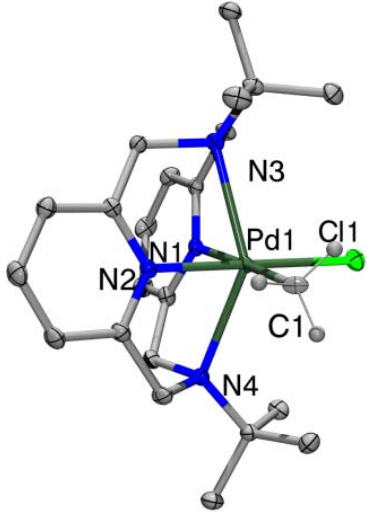
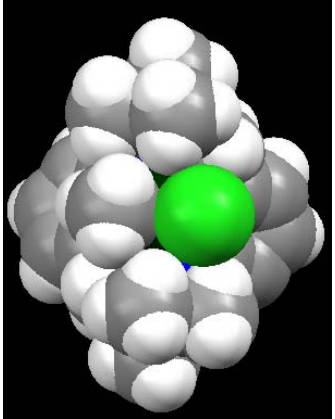
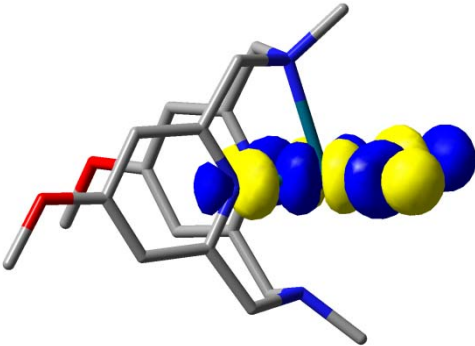
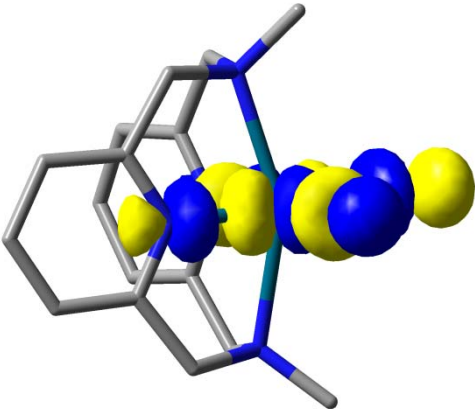
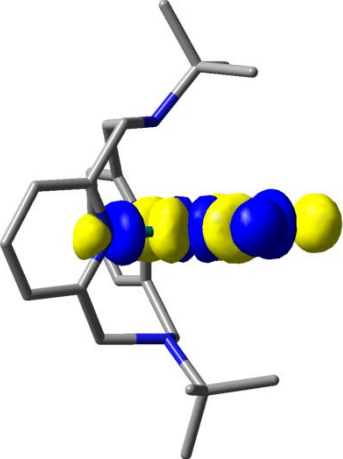
Side view of complexes	Selected bond distances and angles	Space filling model for the front view of complexes
<p><math>[(^{\text{Me}}\text{N}4^{\text{OMe}})\text{Pd}^{\text{III}}\text{MeCl}]^+ (4^+)</math></p> 	<p>Pd1-N1 2.055(3) Å  Pd1-N2 2.130(3) Å  Pd1-N3 2.297(3) Å  Pd1-N4 2.340(3) Å  Pd1-C1 2.040(4) Å  Pd1-Cl1 2.3298(11) Å</p> <p>N1-Pd1-N2 81.09(12)°  N3-Pd1-N4 149.19(11)°</p>	
<p><math>[(^{\text{Me}}\text{N}4)\text{Pd}^{\text{III}}\text{MeCl}]^+ (5^+)</math></p> 	<p>Pd1-N1 2.085(2) Å  Pd1-N1_i 2.085(2) Å  Pd1-N3 2.302(3) Å  Pd1-N4 2.338(3) Å  Pd1-C1 2.021(11) Å  Pd1-Cl1_i 2.344(3) Å</p> <p>N1-Pd1-N1_i 81.44(12)°  N3-Pd1-N4 149.12(11)°</p>	
<p><math>[(^{\text{tBu}}\text{N}4)\text{Pd}^{\text{III}}\text{MeCl}]^+ (6^+)</math></p> 	<p>Pd1-N1 2.0966(16) Å  Pd1-N2 2.0204(16) Å  Pd1-N3 2.4271(16) Å  Pd1-N4 2.4265(16) Å  Pd1-C1 2.0921(18) Å  Pd1-Cl1 2.3403(5) Å</p> <p>N1-Pd1-N2 86.61(6)°  N3-Pd1-N4 142.37(5)°</p>	

Figure S26. ORTEP diagrams and space filling models of  $[(^{\text{R}}\text{N}4)\text{Pd}^{\text{III}}\text{MeCl}]^+$  complexes.

## VII. Computational Details

The density functional theory (DFT) calculations were performed with the program package Gaussian 09. Single point and geometry optimization calculations were performed using the B3LYP functional,<sup>7,8</sup> along with the Stevens CEP-31G(d) valence basis sets with effective core potentials.<sup>9,10</sup> The CEP-31G(d) valence basis set is of triple- $\zeta$  for palladium and double- $\zeta$  for main group elements, with an additional d polarization function for Cl. This functional/basis set combination has been shown previously to reproduce well experimental parameters of Pd complexes.<sup>11,12</sup> Single point calculations were performed using the crystallographic coordinates for complexes **1**<sup>+</sup>-**6**<sup>+</sup>, with solvent and counteranion molecules being excluded. The calculated ground state wavefunctions were investigated by analyzing the frontier molecular orbitals and the atomic contributions to the spin density. The atomic orbital contributions to the frontier molecular orbitals were calculated using the program Chemissian.<sup>13</sup> TD-DFT calculations were employed to obtain the predicted absorption bands and their major contributions transitions. The calculated UV-vis spectra were generated using the program GaussSum, with a full width at half maximum (FWHM) value of 3750 cm<sup>-1</sup>.<sup>14</sup>

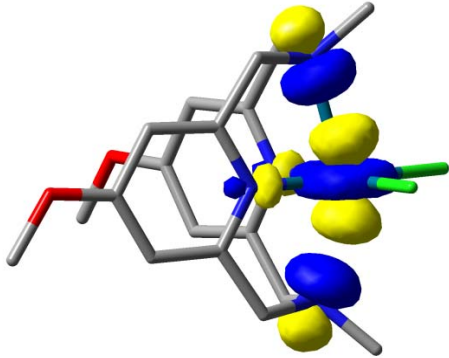
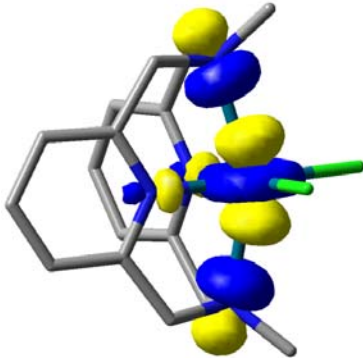
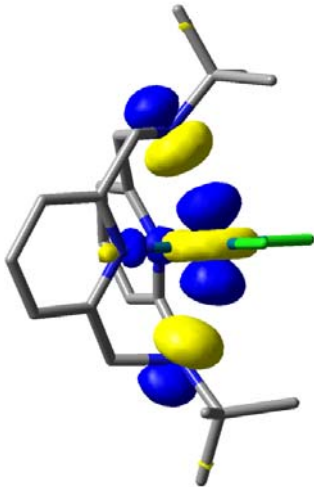
**Table S1.** Comparison of  $\alpha$ -LUMOs of Pd<sup>III</sup> complexes **1**<sup>+</sup>-**3**<sup>+</sup>.

MO # Energy (eV)	MOs (0.05 isocontour value)	Major AO Contributions
$\alpha$ -LUMO of [[ <sup>Me</sup> N4 <sup>OMe</sup> ]Pd <sup>III</sup> Cl <sub>2</sub> ] <sup>+</sup> Energy: -3.641		Pd      26 % N <sub>axial</sub> 0 % N <sub>eq</sub> 24 % Cl      22 %
$\alpha$ -LUMO of [[ <sup>Me</sup> N4]Pd <sup>III</sup> Cl <sub>2</sub> ] <sup>+</sup> Energy: -3.731		Pd      27 % N <sub>axial</sub> 0 % N <sub>eq</sub> 26 % Cl      24 %
$\alpha$ -LUMO of [[ <sup>tBu</sup> N4]Pd <sup>III</sup> Cl <sub>2</sub> ] <sup>+</sup> Energy: -3.624		Pd      27 % N <sub>axial</sub> 0 % N <sub>eq</sub> 28 % Cl      22 %

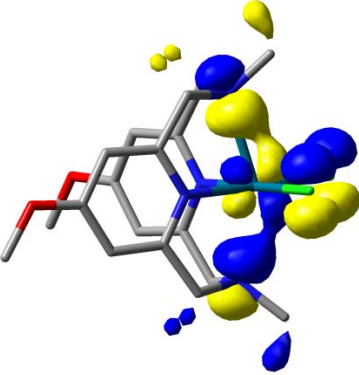
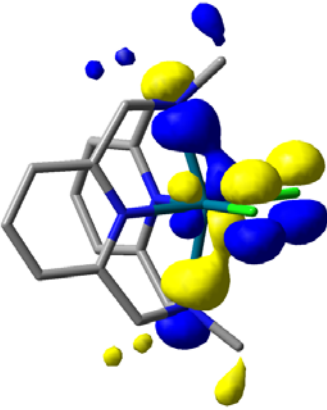
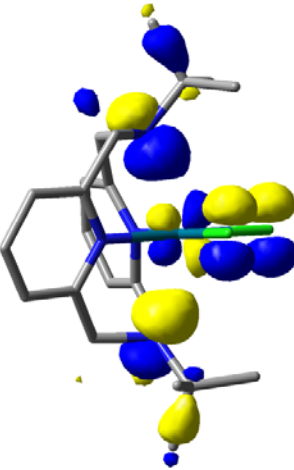
**Table S2.** Comparison of  $\alpha$ -HOMOs of Pd<sup>III</sup> complexes **1**<sup>+</sup>-**3**<sup>+</sup>.

MO # Energy (eV)	MOs (0.05 isocontour value)	Major AO Contributions
$\alpha$ -HOMO of [[ <sup>Me</sup> N4 <sup>OMe</sup> ]Pd <sup>III</sup> Cl <sub>2</sub> ] <sup>+</sup> Energy: -6.416		Pd      27 % N <sub>axial</sub> 44 % N <sub>eq</sub> 6 % Cl          6 %
$\alpha$ -HOMO of [[ <sup>Me</sup> N4]Pd <sup>III</sup> Cl <sub>2</sub> ] <sup>+</sup> Energy: -6.460		Pd      27% N <sub>axial</sub> 44 % N <sub>eq</sub> 6 % Cl          6 %
$\alpha$ -HOMO of [[ <sup>tBu</sup> N4]Pd <sup>III</sup> Cl <sub>2</sub> ] <sup>+</sup> Energy: -6.687		Pd      23 % N <sub>axial</sub> 42 % N <sub>eq</sub> 6 % Cl          6 %

**Table S3.** Comparison of  $\beta$ -LUMOs of Pd<sup>III</sup> complexes **1**<sup>+</sup>-**3**<sup>+</sup>.

MO # Energy (eV)	MOs (0.05 isocontour value)	Major AO Contributions
$\beta$ -LUMO of [( <sup>Me</sup> N4 <sup>OMe</sup> )Pd <sup>III</sup> Cl <sub>2</sub> ] <sup>+</sup> Energy: -3.753		Pd      35 % N <sub>axial</sub> 36 % N <sub>eq</sub> 6 % Cl          4 %
$\beta$ -LUMO of [( <sup>Me</sup> N4)Pd <sup>III</sup> Cl <sub>2</sub> ] <sup>+</sup> Energy: -3.798		Pd      35 % N <sub>axial</sub> 36 % N <sub>eq</sub> 6 % Cl          4 %
$\beta$ -LUMO of [( <sup>tBu</sup> N4)Pd <sup>III</sup> Cl <sub>2</sub> ] <sup>+</sup> Energy: -4.194		Pd      32 % N <sub>axial</sub> 34 % N <sub>eq</sub> 6 % Cl          4 %

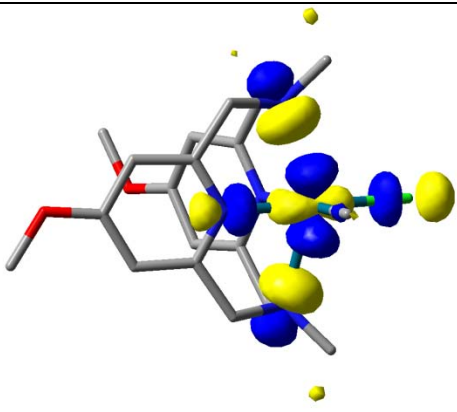
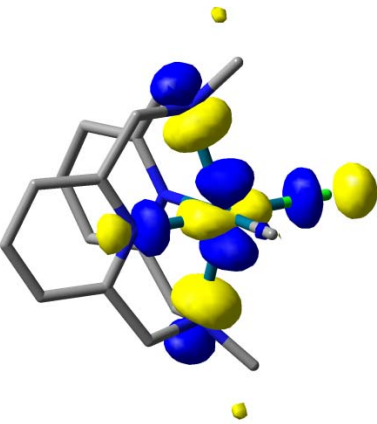
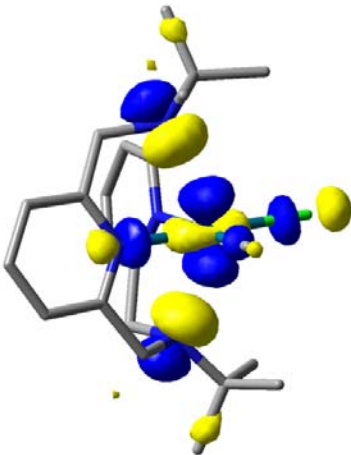
**Table S4.** Comparison of  $\beta$ -HOMOs of Pd<sup>III</sup> complexes **1**<sup>+</sup>-**3**<sup>+</sup>.

MO # Energy (eV)	MOs (0.05 isocontour value)	Major AO Contributions
$\beta$ -HOMO of [[ <sup>Me</sup> N4 <sup>OMe</sup> ] <sup>+</sup> Pd <sup>III</sup> Cl <sub>2</sub> ] <sup>+</sup> Energy: -7.198		Pd      14 % N <sub>axial</sub> 42 % Cl        24 %
$\beta$ -HOMO of [[ <sup>Me</sup> N4] <sup>+</sup> Pd <sup>III</sup> Cl <sub>2</sub> ] <sup>+</sup> Energy: -7.252		Pd      14 % N <sub>axial</sub> 42 % Cl        24 %
$\beta$ -HOMO of [[ <sup>tBu</sup> N4] <sup>+</sup> Pd <sup>III</sup> Cl <sub>2</sub> ] <sup>+</sup> Energy: -6.903		Pd      9 % N <sub>axial</sub> 39 % Cl        17 %

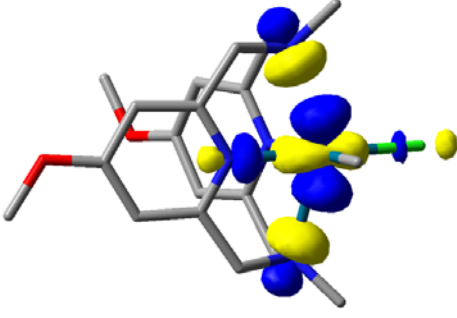
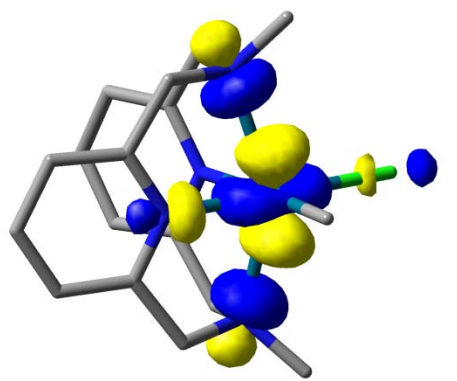
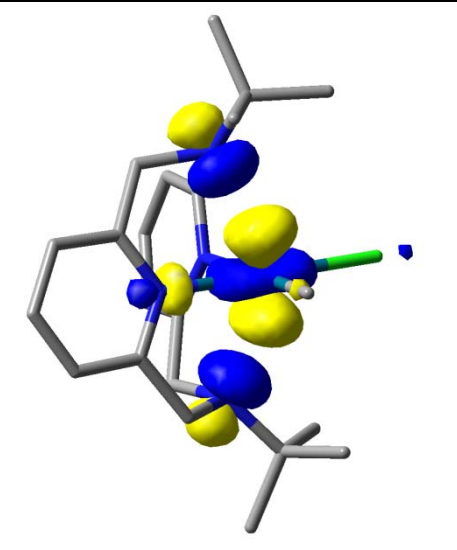
**Table S5.** Comparison of  $\alpha$ -LUMOs of Pd<sup>III</sup> complexes **4**<sup>+</sup>-**6**<sup>+</sup>.

MO # Energy (eV)	MOs (0.05 isocontour value)	Major AO Contributions
$\alpha$ -LUMO of [( <sup>Me</sup> N4 <sup>OMe</sup> )Pd <sup>III</sup> MeCl] <sup>+</sup> Energy: -2.213		Pd 23 % N <sub>eq</sub> 14 % Cl 10 % C 25%
$\alpha$ -LUMO of [( <sup>Me</sup> N4)Pd <sup>III</sup> MeCl] <sup>+</sup> Energy: -2.304		Pd 21 % N <sub>eq</sub> 16 % Cl 10 % C(39) 22 %
$\alpha$ -LUMO of [( <sup>tBu</sup> N4)Pd <sup>III</sup> MeCl] <sup>+</sup> Energy: -2.302		Pd 20 % N <sub>eq</sub> 20 % Cl 8 % C(7) 19 %

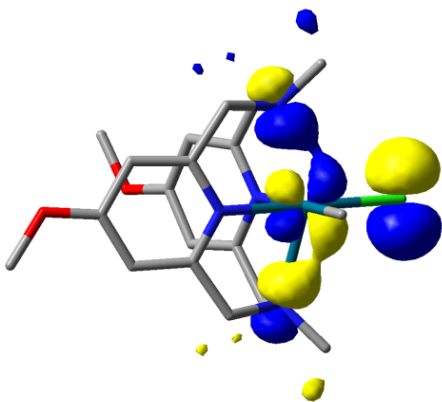
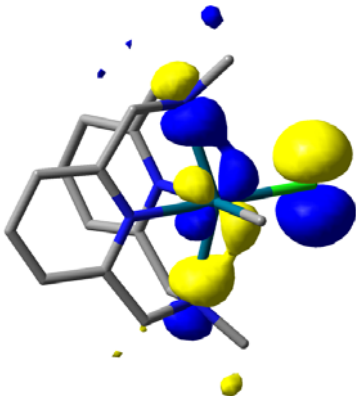
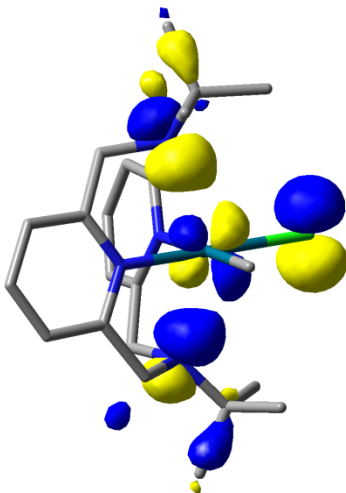
**Table S6.** Comparison of  $\alpha$ -HOMOs of Pd<sup>III</sup> complexes 4<sup>+</sup>-6<sup>+</sup>.

MO # Energy (eV)	MOs (0.05 isocontour value)	Major Contributions	AO
$\alpha$ -HOMO of [[ <sup>Me</sup> N4 <sup>OMe</sup> ]Pd <sup>III</sup> MeCl] <sup>+</sup> Energy: -5.984		Pd 29 % N <sub>axial</sub> 38 % N <sub>eq</sub> 7 % Cl 8 %	
$\alpha$ -HOMO [[ <sup>Me</sup> N4]Pd <sup>III</sup> MeCl] <sup>+</sup> Energy: -6.022		Pd 29 % N <sub>axial</sub> 38 % N <sub>eq</sub> 8 % Cl 8 %	
$\alpha$ -HOMO of [[ <sup>tBu</sup> N4]Pd <sup>III</sup> MeCl] <sup>+</sup> Energy: -6.261		Pd 26 % N <sub>axial</sub> 38 % N <sub>eq</sub> 6 % Cl 6 %	

**Table S7.** Comparison of  $\beta$ -LUMOs of Pd<sup>III</sup> complexes 4<sup>+</sup>-6<sup>+</sup>.

MO # Energy (eV)	MOs (0.05 isocontour value)	Major AO Contributions
$\beta$ -LUMO of [( <sup>Me</sup> N4 <sup>OMe</sup> )Pd <sup>III</sup> MeCl] <sup>+</sup> Energy: -3.211		Pd 37 % N <sub>axial</sub> 30 % N <sub>eq</sub> 6 % Cl 4 %
$\beta$ -LUMO of [( <sup>Me</sup> N4)Pd <sup>III</sup> MeCl] <sup>+</sup> Energy: -3.247		Pd 37 % N <sub>axial</sub> 30 % N <sub>eq</sub> 6 % Cl 5 %
$\beta$ -LUMO of [( <sup>tBu</sup> N4)Pd <sup>III</sup> MeCl] <sup>+</sup> Energy: -3.634		Pd 37 % N <sub>axial</sub> 29 % N <sub>eq</sub> 5 % Cl 3 %

**Table S8.** Comparison of  $\beta$ -HOMOs of Pd<sup>III</sup> complexes **4**<sup>+</sup>-**6**<sup>+</sup>.

MO # Energy (eV)	MOs (0.05 isocontour value)	Major AO Contributions
$\beta$ -HOMO of [[ <sup>Me</sup> N4 <sup>OMe</sup> )Pd <sup>III</sup> MeCl] <sup>+</sup> Energy: -6.901		Pd 21 % N <sub>axial</sub> 32 % Cl 28 %
$\beta$ -HOMO [[ <sup>Me</sup> N4)Pd <sup>III</sup> MeCl] <sup>+</sup> Energy: -6.950		Pd 21 % N <sub>axial</sub> 32 % Cl 30 %
$\beta$ -HOMO of [[ <sup>tBu</sup> N4)Pd <sup>III</sup> MeCl] <sup>+</sup> Energy: -6.710		Pd 12 % N <sub>axial</sub> 37 % Cl 16 %

**Table S9.** TD-DFT calculated absorption bands and their composition for  $[(\text{MeN4OMe})\text{Pd}^{\text{III}}\text{Cl}_2]^+$  ( $1^+$ ). Only the transitions with oscillator strengths greater than 0.005 are listed; and only the major contributing transitions with more than 10% contribution are shown.

Wavelength (nm)	Oscillator strength	Major contributing transitions
605.44	0.043	$\beta$ -HOMO $\rightarrow$ $\beta$ -LUMO (86%)
395.44	0.009	$\alpha$ -HOMO-5 $\rightarrow$ $\alpha$ -LUMO (49%), $\alpha$ -HOMO-1 $\rightarrow$ $\alpha$ -LUMO (12%), $\beta$ -HOMO-1 $\rightarrow$ $\beta$ -LUMO+1 (32%)
377.99	0.007	$\alpha$ -HOMO-6 $\rightarrow$ $\alpha$ -LUMO (16%), $\beta$ -HOMO-7 $\rightarrow$ $\beta$ -LUMO (65%)
375.33	0.022	$\alpha$ -HOMO-6 $\rightarrow$ $\alpha$ -LUMO (69%), $\beta$ -HOMO-7 $\rightarrow$ $\beta$ -LUMO (15%)
357.58	0.027	$\beta$ -HOMO-4 $\rightarrow$ $\beta$ -LUMO+1 (58%), $\beta$ -HOMO-1 $\rightarrow$ $\beta$ -LUMO+1 (23%)
345.39	0.007	$\beta$ -HOMO-8 $\rightarrow$ $\beta$ -LUMO (16%), $\beta$ -HOMO-5 $\rightarrow$ $\beta$ -LUMO+1 (73%)
308.85	0.008	$\alpha$ -HOMO-15 $\rightarrow$ $\alpha$ -LUMO (25%), $\beta$ -HOMO-14 $\rightarrow$ $\beta$ -LUMO (13%), $\beta$ -HOMO-13 $\rightarrow$ $\beta$ -LUMO (12%)
301.68	0.011	$\alpha$ -HOMO-15 $\rightarrow$ $\alpha$ -LUMO (24%), $\beta$ -HOMO-14 $\rightarrow$ $\beta$ -LUMO (26%), $\beta$ -HOMO-13 $\rightarrow$ $\beta$ -LUMO (25%)

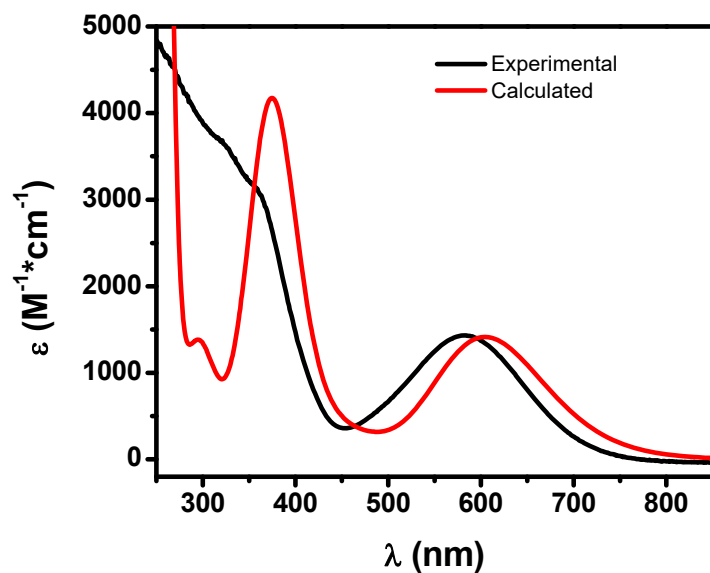


*Figure S27.* UV-vis spectra of  $[(\text{MeN4OMe})\text{Pd}^{\text{III}}\text{Cl}_2]^+$  ( $1^+$ ): experimental spectrum in MeCN (black line), and TD-DFT calculated UV-vis spectrum (red line).

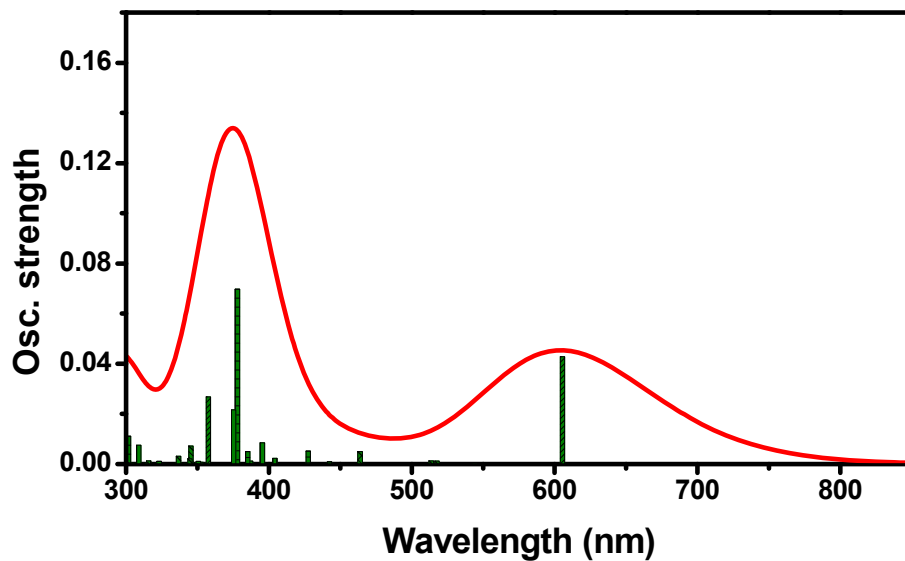


*Figure S28.* TD-DFT calculated UV-vis spectrum of  $[(\text{MeN4OMe})\text{Pd}^{\text{III}}\text{Cl}_2]^+$  ( $1^+$ ).

**Table S10.** TD-DFT calculated absorption bands and their composition for  $[(\text{MeN}4)\text{Pd}^{\text{III}}\text{Cl}_2]^+ (2^+)$ . Only the transitions with oscillator strengths greater than 0.005 are listed; and only the major contributing transitions with more than 10% contribution are shown.

<b>Wavelength (nm)</b>	<b>Oscillator strength</b>	<b>Major contributing transitions</b>
600.99	0.042	$\beta\text{-HOMO} \rightarrow \beta\text{-LUMO}$ (85%), $\beta\text{-HOMO-13} \rightarrow \beta\text{-LUMO}$ (8%)
404.67	0.006	$\alpha\text{-HOMO-1} \rightarrow \alpha\text{-LUMO}$ (16%), $\beta\text{-HOMO-2} \rightarrow \beta\text{-LUMO+1}$ (82%)
378.83	0.009	$\beta\text{-HOMO-6} \rightarrow \beta\text{-LUMO}$ (16%), $\beta\text{-HOMO-5} \rightarrow \beta\text{-LUMO}$ (73%)
343.90	0.006	$\beta\text{-HOMO-6} \rightarrow \beta\text{-LUMO}$ (74%), $\beta\text{-HOMO-5} \rightarrow \beta\text{-LUMO}$ (17%)
302.28	0.007	$\alpha\text{-HOMO-13} \rightarrow \alpha\text{-LUMO}$ (12%), $\beta\text{-HOMO-13} \rightarrow \beta\text{-LUMO}$ (39%), $\beta\text{-HOMO} \rightarrow \beta\text{-LUMO+2}$ (37%)

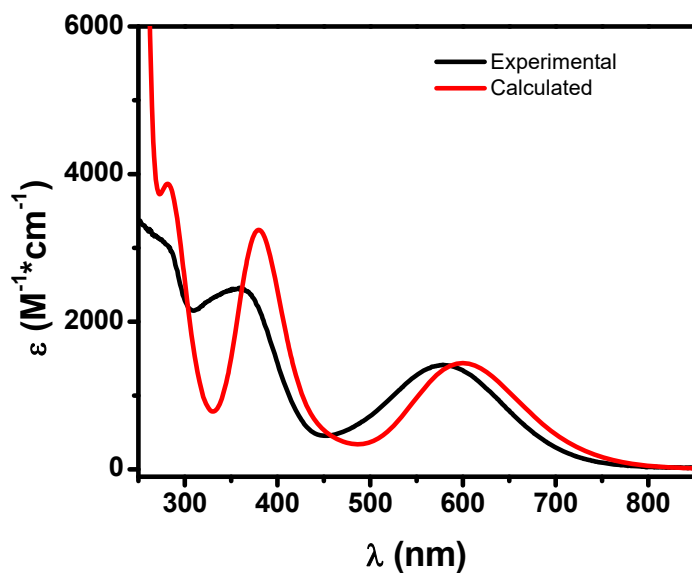


**Figure S29.** UV-vis spectra of  $[(\text{Me}_4\text{N})\text{Pd}^{\text{III}}\text{Cl}_2]^+$  ( $2^+$ ): experimental spectrum in MeCN (black line), and TD-DFT calculated UV-vis spectrum (red line).

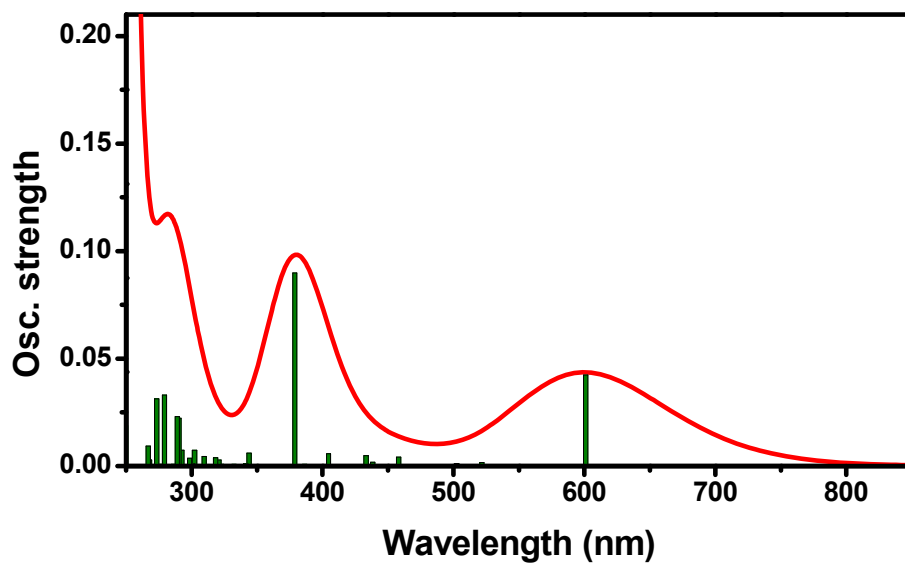


**Figure S30.** TD-DFT calculated UV-vis spectrum of  $[(\text{Me}_4\text{N})\text{Pd}^{\text{III}}\text{Cl}_2]^+$  ( $1^+$ ).

**Table S11.** TD-DFT calculated absorption bands and their composition for  $[(^t\text{BuN}_4)\text{Pd}^{\text{III}}\text{Cl}_2]^+$  ( $3^+$ ). Only the transitions with oscillator strengths greater than 0.005 are listed; and only the major contributing transitions with more than 10% contribution are shown.

Wavelength (nm)	Oscillator strength	Major contributing transitions
806.47	0.066	$\beta\text{-HOMO} \rightarrow \beta\text{-LUMO}$ (89%)
471.19	0.055	$\beta\text{-HOMO-6} \rightarrow \beta\text{-LUMO}$ (28%), $\beta\text{-HOMO-4} \rightarrow \beta\text{-LUMO}$ (56%)
440.94	0.037	$\beta\text{-HOMO-6} \rightarrow \beta\text{-LUMO}$ (48%), $\beta\text{-HOMO-4} \rightarrow \beta\text{-LUMO}$ (35%)
355.75	0.013	$\alpha\text{-HOMO-6} \rightarrow \alpha\text{-LUMO}$ (13%), $\beta\text{-HOMO-18} \rightarrow \beta\text{-LUMO}$ (14%), $\beta\text{-HOMO-14} \rightarrow \beta\text{-LUMO}$ (13%), $\beta\text{-HOMO-11} \rightarrow \beta\text{-LUMO}$ (20%)
335.81	0.006	$\alpha\text{-HOMO-8} \rightarrow \alpha\text{-LUMO}$ (41%), $\beta\text{-HOMO-8} \rightarrow \beta\text{-LUMO+1}$ (10%), $\beta\text{-HOMO-7} \rightarrow \beta\text{-LUMO+1}$ (12%)
315.04	0.008	$\alpha\text{-HOMO-10} \rightarrow \alpha\text{-LUMO}$ (63%), $\beta\text{-HOMO-8} \rightarrow \beta\text{-LUMO+1}$ (12%)
302.24	0.010	$\alpha\text{-HOMO-8} \rightarrow \alpha\text{-LUMO}$ (17%), $\beta\text{-HOMO-7} \rightarrow \beta\text{-LUMO+1}$ (35%),

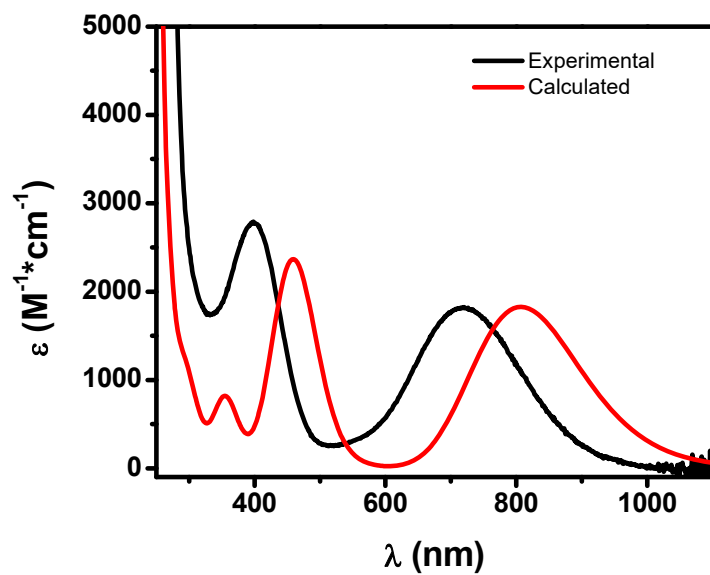


*Figure S31.* UV-vis spectra of  $[(\text{tBuN}_4)\text{Pd}^{\text{III}}\text{Cl}_2]^+$  ( $3^+$ ): experimental spectrum in MeCN (black line), and TD-DFT calculated UV-vis spectrum (red line).

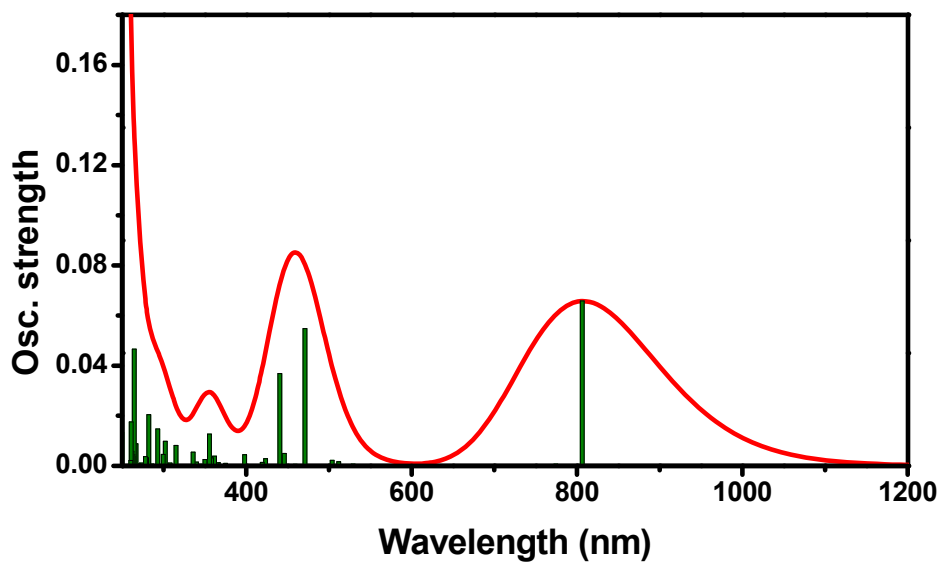


*Figure S32.* TD-DFT calculated UV-vis spectrum of  $[(\text{tBuN}_4)\text{Pd}^{\text{III}}\text{Cl}_2]^+$  ( $3^+$ ).

**Table S12.** TD-DFT calculated absorption bands and their composition for  $[(\text{MeN}_4\text{OMe})\text{Pd}^{\text{III}}\text{MeCl}]^+$  ( $4^+$ ). Only the transitions with oscillator strengths greater than 0.005 are listed; and only the major contributing transitions with more than 10% contribution are shown.

Wavelength (nm)	Oscillator strength	Major contributing transitions
635.88	0.018	$\beta$ -HOMO $\rightarrow$ $\beta$ -LUMO (82%), $\beta$ -HOMO-12 $\rightarrow$ $\beta$ -LUMO (14%)
494.31	0.007	$\beta$ -HOMO-9 $\rightarrow$ $\beta$ -LUMO (36%), $\beta$ -HOMO-5 $\rightarrow$ $\beta$ -LUMO (27%), $\beta$ -HOMO-4 $\rightarrow$ $\beta$ -LUMO (25%),
370.63	0.006	$\alpha$ -HOMO $\rightarrow$ $\alpha$ -LUMO+1 (55%), $\beta$ -HOMO-2 $\rightarrow$ $\beta$ -LUMO (25%)
347.26	0.029	$\alpha$ -HOMO $\rightarrow$ $\alpha$ -LUMO+2 (25%), $\beta$ -HOMO-9 $\rightarrow$ $\beta$ -LUMO (28%), $\beta$ -HOMO-5 $\rightarrow$ $\beta$ -LUMO (13%), $\beta$ -HOMO-4 $\rightarrow$ $\beta$ -LUMO (12%)
344.67	0.013	$\alpha$ -HOMO $\rightarrow$ $\alpha$ -LUMO+2 (71%)
335.39	0.010	$\alpha$ -HOMO-1 $\rightarrow$ $\alpha$ -LUMO (34%), $\beta$ -HOMO-1 $\rightarrow$ $\beta$ -LUMO+1 (35%)
334.39	0.029	$\alpha$ -HOMO-2 $\rightarrow$ $\alpha$ -LUMO (33%), $\beta$ -HOMO $\rightarrow$ $\beta$ -LUMO+1 (15%)
330.66	0.013	$\beta$ -HOMO-7 $\rightarrow$ $\beta$ -LUMO (28%), $\beta$ -HOMO-6 $\rightarrow$ $\beta$ -LUMO
324.41	0.009	$\alpha$ -HOMO-10 $\rightarrow$ $\alpha$ -LUMO (13%), $\alpha$ -HOMO-6 $\rightarrow$ $\alpha$ -LUMO (20%), $\alpha$ -HOMO-2 $\rightarrow$ $\alpha$ -LUMO (11%), $\beta$ -HOMO $\rightarrow$ $\beta$ -LUMO+1 (18%)
322.38	0.014	$\beta$ -HOMO-12 $\rightarrow$ $\beta$ -LUMO (61%), $\beta$ -HOMO $\rightarrow$ $\beta$ -LUMO
314.70	0.019	$\beta$ -HOMO-8 $\rightarrow$ $\beta$ -LUMO (67%),

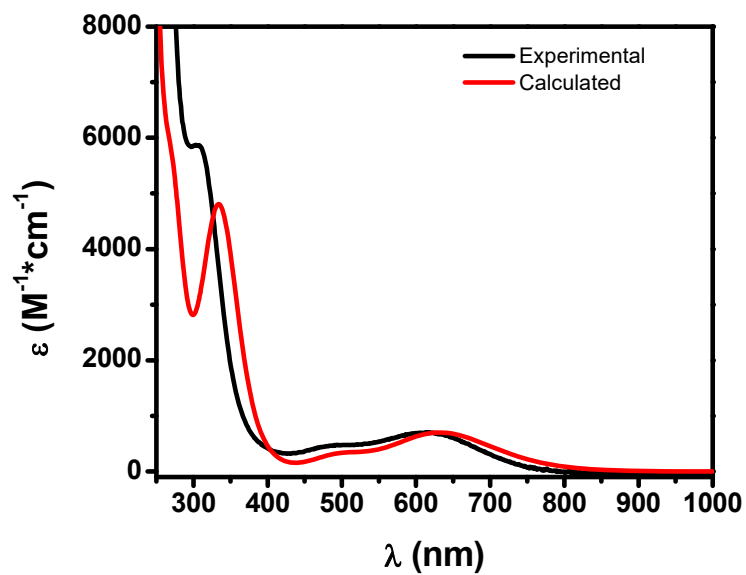


*Figure S33.* UV-vis spectra of  $[(\text{Me}_4\text{N})\text{Pd}^{\text{III}}\text{MeCl}]^+$  ( $4^+$ ): experimental spectrum in MeCN (black line), and TD-DFT calculated UV-vis spectrum (red line).

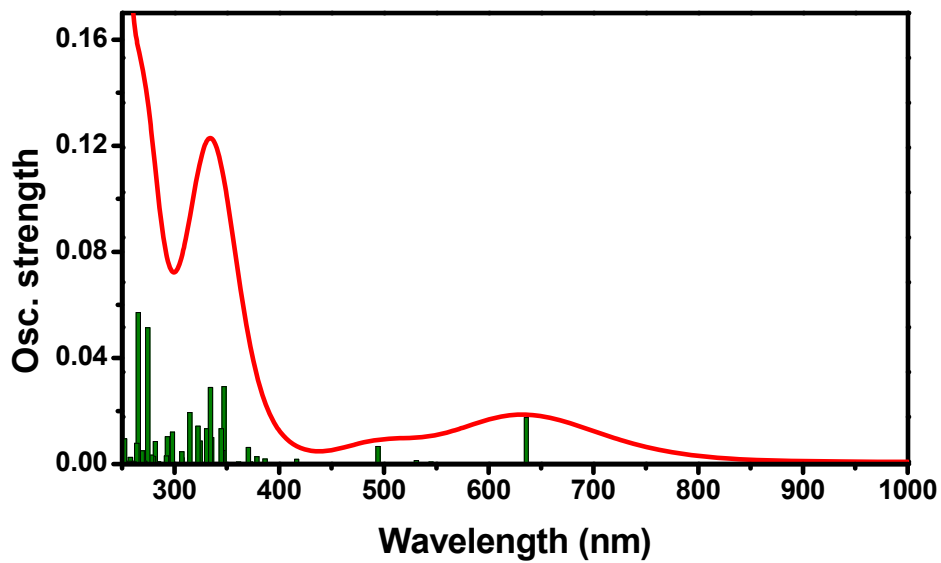


*Figure S34.* TD-DFT calculated UV-vis spectrum of  $[(\text{Me}_4\text{N})\text{Pd}^{\text{III}}\text{MeCl}]^+$  ( $4^+$ ).

**Table S13.** TD-DFT calculated absorption bands and their composition for  $[(\text{MeN}_4)\text{Pd}^{\text{III}}\text{MeCl}]^+ (5^+)$ . Only the transitions with oscillator strengths greater than 0.005 are listed; and only the major contributing transitions with more than 10% contribution are shown.

Wavelength (nm)	Oscillator strength	Major contributing transitions
629.29	0.017	$\beta\text{-HOMO} \rightarrow \beta\text{-LUMO}$ (82%), $\beta\text{-HOMO-11} \rightarrow \beta\text{-LUMO}$ (14%)
488.91	0.007	$\beta\text{-HOMO-8} \rightarrow \beta\text{-LUMO}$ (36%), $\beta\text{-HOMO-3} \rightarrow \beta\text{-LUMO}$ (50%),
347.35	0.038	$\beta\text{-HOMO-8} \rightarrow \beta\text{-LUMO}$ (35%), $\beta\text{-HOMO-3} \rightarrow \beta\text{-LUMO}$ (33%)
336.20	0.030	$\alpha\text{-HOMO-1} \rightarrow \alpha\text{-LUMO}$ (32%)
331.28	0.016	$\alpha\text{-HOMO-2} \rightarrow \alpha\text{-LUMO}$ (27%), $\beta\text{-HOMO-6} \rightarrow \beta\text{-LUMO}$ (14%), $\beta\text{-HOMO-1} \rightarrow \beta\text{-LUMO+1}$ (12%), $\beta\text{-HOMO-1} \rightarrow \beta\text{-LUMO+2}$ (16%)
325.93	0.006	$\alpha\text{-HOMO-10} \rightarrow \alpha\text{-LUMO}$ (12%), $\alpha\text{-HOMO-4} \rightarrow \alpha\text{-LUMO}$ (15%), $\beta\text{-HOMO-3} \rightarrow \beta\text{-LUMO+2}$ (12%),
314.30	0.013	$\beta\text{-HOMO-11} \rightarrow \beta\text{-LUMO}$ (24%), $\beta\text{-HOMO-5} \rightarrow \beta\text{-LUMO}$ (32%)
312.62	0.041	$\beta\text{-HOMO-7} \rightarrow \beta\text{-LUMO}$ (52%), $\beta\text{-HOMO-6} \rightarrow \beta\text{-LUMO}$ (32%)

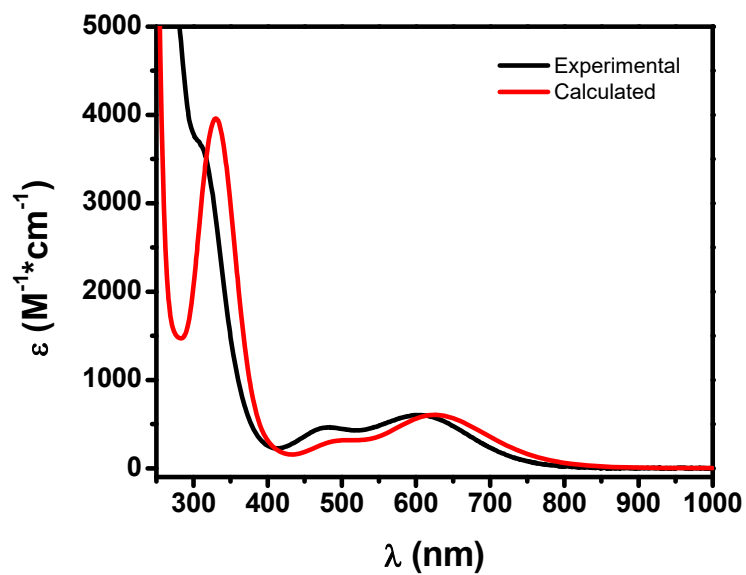


**Figure S35.** UV-vis spectra of  $[(\text{Me}_4\text{N})\text{Pd}^{\text{III}}\text{MeCl}]^+$  (5<sup>+</sup>): experimental spectrum in MeCN (black line), and TD-DFT calculated UV-vis spectrum (red line).

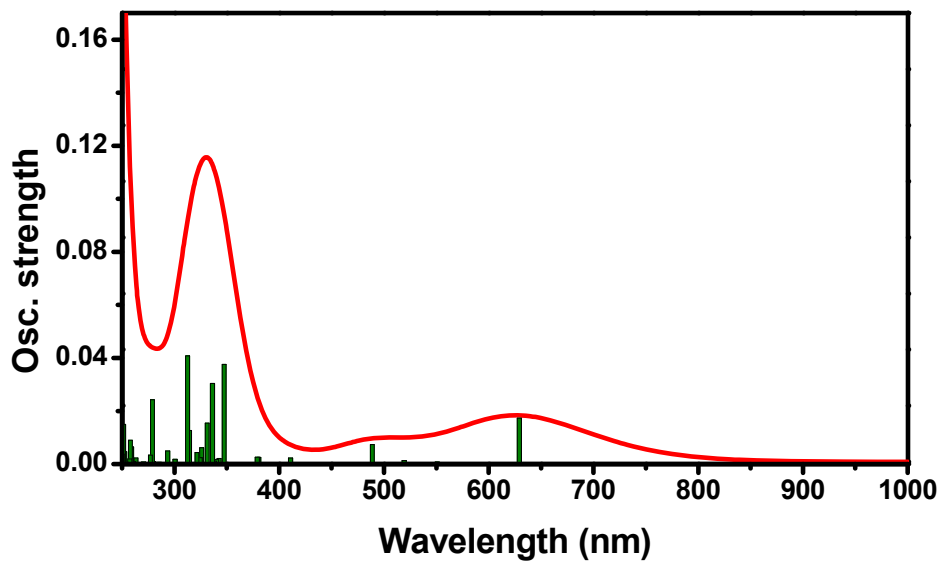


**Figure S36.** TD-DFT calculated UV-vis spectrum of  $[(\text{Me}_4\text{N})\text{Pd}^{\text{III}}\text{MeCl}]^+$  (5<sup>+</sup>).

**Table S14.** TD-DFT calculated absorption bands and their composition for  $[(^t\text{BuN}_4)\text{Pd}^{\text{III}}\text{MeCl}]^+$  ( $6^+$ ). Only the transitions with oscillator strengths greater than 0.005 are listed; and only the major contributing transitions with more than 10% contribution are shown.

Wavelength (nm)	Oscillator strength	Major contributing transitions
775.53	0.033	$\beta$ -HOMO $\rightarrow$ $\beta$ -LUMO (81%), $\beta$ -HOMO-11 $\rightarrow$ $\beta$ -LUMO (9%),
564.84	0.010	$\beta$ -HOMO-9 $\rightarrow$ $\beta$ -LUMO (20%), $\beta$ -HOMO-3 $\rightarrow$ $\beta$ -LUMO (22%), $\beta$ -HOMO-2 $\rightarrow$ $\beta$ -LUMO (30%)
422.27	0.058	$\beta$ -HOMO-9 $\rightarrow$ $\beta$ -LUMO (24%), $\beta$ -HOMO-2 $\rightarrow$ $\beta$ -LUMO (44%)
398.77	0.034	$\beta$ -HOMO-9 $\rightarrow$ $\beta$ -LUMO (11%), $\beta$ -HOMO-3 $\rightarrow$ $\beta$ -LUMO (56%), $\beta$ -HOMO-2 $\rightarrow$ $\beta$ -LUMO (11%)
371.82	0.008	$\beta$ -HOMO-11 $\rightarrow$ $\beta$ -LUMO (10%), $\beta$ -HOMO-8 $\rightarrow$ $\beta$ -LUMO (14%), $\beta$ -HOMO-6 $\rightarrow$ $\beta$ -LUMO (11%), $\beta$ -HOMO-5 $\rightarrow$ $\beta$ -LUMO (18%)
341.66	0.008	$\beta$ -HOMO-9 $\rightarrow$ $\beta$ -LUMO (10%), $\beta$ -HOMO-7 $\rightarrow$ $\beta$ -LUMO (54%)
337.76	0.018	$\beta$ -HOMO-8 $\rightarrow$ $\beta$ -LUMO (22%), $\beta$ -HOMO-7 $\rightarrow$ $\beta$ -LUMO (24%), $\beta$ -HOMO-6 $\rightarrow$ $\beta$ -LUMO (12%)
333.76	0.009	$\alpha$ -HOMO-6 $\rightarrow$ $\alpha$ -LUMO (12%), $\beta$ -HOMO-8 $\rightarrow$ $\beta$ -LUMO (20%)
328.56	0.019	$\alpha$ -HOMO-2 $\rightarrow$ $\alpha$ -LUMO (29%), $\beta$ -HOMO-1 $\rightarrow$ $\beta$ -LUMO+1 (25%), $\beta$ -HOMO-1 $\rightarrow$ $\beta$ -LUMO+2 (10%)

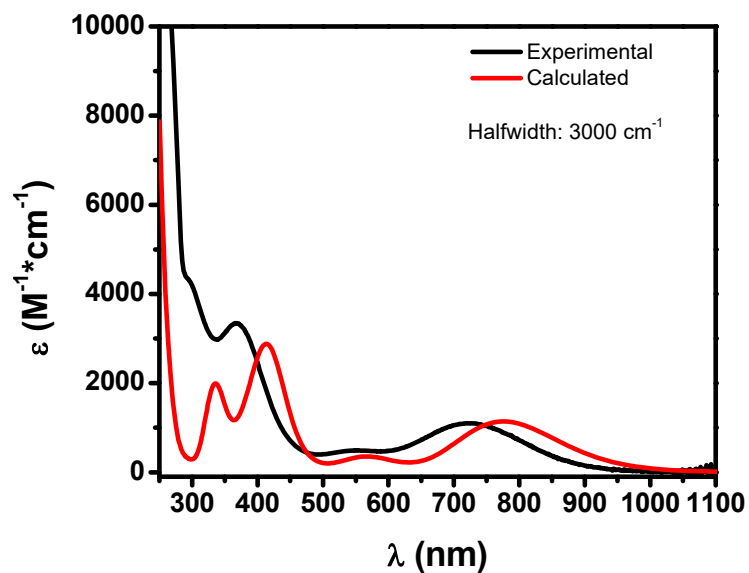


*Figure S37.* UV-vis spectra of  $[(t\text{Bu}_4\text{N})\text{Pd}^{\text{III}}\text{MeCl}]^+$  ( $6^+$ ): experimental spectrum in MeCN (black line), and TD-DFT calculated UV-vis spectrum (red line).

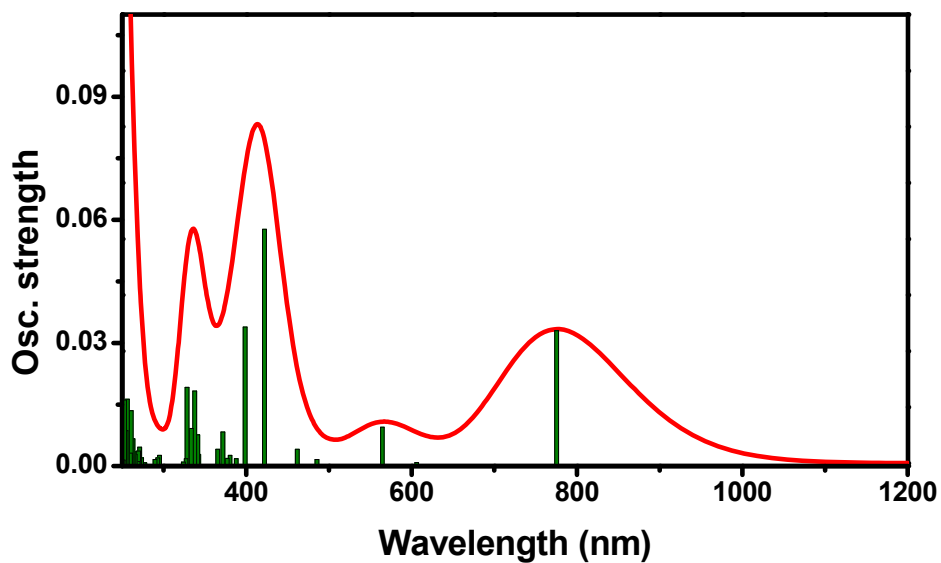


*Figure S38.* TD-DFT calculated UV-vis spectrum of  $[(t\text{Bu}_4\text{N})\text{Pd}^{\text{III}}\text{MeCl}]^+$  ( $6^+$ ).

## VIII. X-ray structure characterization of [1<sup>+</sup>]ClO<sub>4</sub>, [2<sup>+</sup>]ClO<sub>4</sub>, and [4<sup>+</sup>]ClO<sub>4</sub>

*General information:* X-ray quality crystals of [1<sup>+</sup>]ClO<sub>4</sub> and [2<sup>+</sup>]ClO<sub>4</sub> were obtained by slow ether vapor diffusion into the corresponding acetonitrile solutions. Suitable crystals of appropriate dimensions were mounted on Mitgen loops in random orientations. Preliminary examination and data collection were performed using a Bruker Kappa Apex-II Charge Coupled Device (CCD) Detector system single crystal X-Ray diffractometer equipped with an Oxford Cryostream LT device. Data were collected using graphite monochromated Mo K $\alpha$  radiation ( $\lambda = 0.71073 \text{ \AA}$ ) from a fine focus sealed tube X-Ray source. Preliminary unit cell constants were determined with a set of 36 narrow frame scans. Typical data sets consist of a combination of  $\omega$  and  $\phi$  scan frames with typical scan width of  $0.5^\circ$  and counting time of 15-30 seconds/frame at a crystal to detector distance of  $\sim 4.0 \text{ cm}$ . The collected frames were integrated using an orientation matrix determined from the narrow frame scans. Apex II and SAINT software packages (*Bruker Analytical X-Ray, Madison, WI, 2008*) were used for data collection and data integration. Analysis of the integrated data did not show any decay. Final cell constants were determined by global refinement of reflections from the complete data set. Data were corrected for systematic errors using SADABS (*Bruker Analytical X-Ray, Madison, WI, 2008*) based on the Laue symmetry using equivalent reflections.

Structure solutions and refinement were carried out using the SHELXTL-PLUS software package (*Sheldrick, G. M. (2008), Bruker-SHELXTL, Acta Cryst. A64, 112-122*). The structures were refined with full matrix least-squares refinement by minimizing  $\sum w(F_o^2 - F_c^2)^2$ . All non-hydrogen atoms were refined anisotropically to convergence. Typically, H atoms are added at the calculated positions in the final refinement cycles.

Acknowledgement: Funding from the National Science Foundation (MRI, CHE-0420497) for the purchase of the ApexII diffractometer is acknowledged.

**X-ray structure determination of [(<sup>Me</sup>N<sup>OMe</sup>)Pd<sup>III</sup>Cl<sub>2</sub>][ClO<sub>4</sub>], [1<sup>+</sup>][ClO<sub>4</sub>]****Table S15.** Crystal data and structure refinement for lm5112.

Identification code	15112/lt/FT-022112-MeOPdIIICl2	
Empirical formula	C <sub>20</sub> H <sub>27</sub> Cl <sub>3</sub> N <sub>5</sub> O <sub>6</sub> Pd	
Formula weight	646.22	
Temperature	100(2) K	
Wavelength	0.71073 Å	
Crystal system	Monoclinic	
Space group	P2 <sub>1</sub> /m	
Unit cell dimensions	a = 8.0151(7) Å	α = 90°.
	b = 9.9646(10) Å	β = 102.854(4)°.
	c = 16.2762(16) Å	γ = 90°.
Volume	1267.4(2) Å <sup>3</sup>	
Z	2	
Density (calculated)	1.693 Mg/m <sup>3</sup>	
Absorption coefficient	1.094 mm <sup>-1</sup>	
F(000)	654	
Crystal size	0.34 x 0.14 x 0.08 mm <sup>3</sup>	
Theta range for data collection	2.41 to 27.60°.	
Index ranges	-10 ≤ h ≤ 10, -12 ≤ k ≤ 12, -21 ≤ l ≤ 21	
Reflections collected	31010	
Independent reflections	3087 [R(int) = 0.0430]	
Completeness to theta = 27.60°	99.2 %	
Absorption correction	Semi-empirical from equivalents	
Max. and min. transmission	0.9166 and 0.7100	
Refinement method	Full-matrix least-squares on F <sup>2</sup>	
Data / restraints / parameters	3087 / 43 / 207	
Goodness-of-fit on F <sup>2</sup>	1.044	
Final R indices [I > 2σ(I)]	R1 = 0.0269, wR2 = 0.0607	
R indices (all data)	R1 = 0.0349, wR2 = 0.0656	
Largest diff. peak and hole	0.813 and -0.570 e.Å <sup>-3</sup>	

**Table S16.** Bond lengths [Å] for lm5112.

Pd(1)-N(1)#1	2.0009(18)	C(10)-H(10A)	0.9800
Pd(1)-N(1)	2.0009(19)	C(10)-H(10B)	0.9800
Pd(1)-N(2)	2.300(3)	C(10)-H(10C)	0.9800
Pd(1)-Cl(1)	2.3018(6)	C(10A)-H(10D)	0.9800
Pd(1)-Cl(1)#1	2.3018(6)	C(10A)-H(10E)	0.9800
Pd(1)-N(3)	2.308(3)	C(10A)-H(10F)	0.9800
O(1)-C(3)	1.340(3)	N(1S)-C(1S)	1.145(6)
O(1)-C(10)	1.465(5)	C(1S)-C(2S)	1.462(7)
O(1)-C(10A)	1.476(7)	C(2S)-H(2SA)	0.9800
N(3)-C(9)	1.468(4)	C(2S)-H(2SB)	0.9800
N(3)-C(7)	1.475(3)	C(2S)-H(2SC)	0.9800
N(3)-C(7)#1	1.475(3)	Cl(2)-O(4)#2	1.387(5)
N(1)-C(1)	1.344(3)	Cl(2)-O(4)	1.387(5)
N(1)-C(5)	1.351(3)	Cl(2)-O(4B)	1.391(13)
N(2)-C(8)	1.476(5)	Cl(2)-O(3A)#2	1.441(7)
N(2)-C(6)#1	1.479(3)	Cl(2)-O(2A)	1.441(8)
N(2)-C(6)	1.479(3)	Cl(2)-O(3A)	1.441(7)
C(1)-C(2)	1.374(3)	Cl(2)-O(2A)#2	1.441(8)
C(1)-C(7)	1.503(3)	Cl(2)-O(4A)#2	1.453(5)
C(2)-C(3)	1.385(4)	Cl(2)-O(4A)	1.453(5)
C(2)-H(2)	0.9500	Cl(2)-O(2)	1.454(12)
C(3)-C(4)	1.394(4)	Cl(2)-O(3)	1.465(12)
C(4)-C(5)	1.370(3)		
C(4)-H(4)	0.9500		
C(5)-C(6)	1.500(3)		
C(6)-H(6A)	0.9900		
C(6)-H(6B)	0.9900		
C(7)-H(7A)	0.9900		
C(7)-H(7B)	0.9900		
C(8)-H(8A)	0.980(3)		
C(8)-H(8B)	0.980(3)		
C(9)-H(9A)	0.980(3)		
C(9)-H(9B)	0.980(3)		

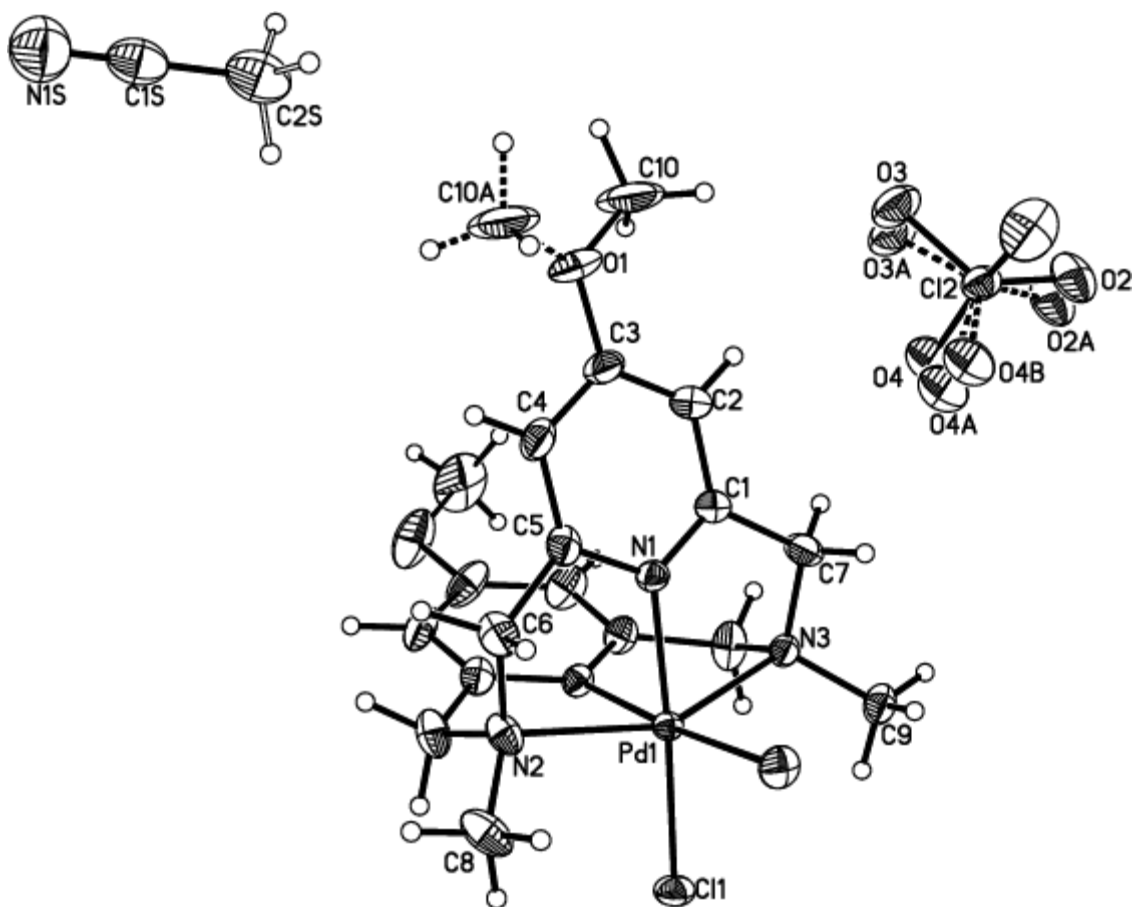


**Figure S39.** Projection view of  $[1^+]\text{ClO}_4$  with 50% thermal ellipsoids.

**X-ray structure determination of [(<sup>Me</sup>N<sub>4</sub>)Pd<sup>III</sup>Cl<sub>2</sub>]ClO<sub>4</sub>, [2<sup>+</sup>]ClO<sub>4</sub>**

**Table S17.** Crystal data and structure refinement for lm24010

Identification code	124010t4/lt/FT-102210-PdIIICl2	
Empirical formula	C <sub>16</sub> H <sub>20</sub> Cl <sub>3</sub> N <sub>4</sub> O <sub>4</sub> Pd	
Formula weight	545.11	
Temperature	100(2) K	
Wavelength	0.71073 Å	
Crystal system	Monoclinic	
Space group	P2 <sub>1</sub> /c	
Unit cell dimensions	a = 12.0665(17) Å	α = 90°.
	b = 11.2092(17) Å	β = 100.331(6)°.
	c = 14.860(2) Å	γ = 90°.
Volume	1977.3(5) Å <sup>3</sup>	
Z	4	
Density (calculated)	1.831 Mg/m <sup>3</sup>	
Absorption coefficient	1.375 mm <sup>-1</sup>	
F(000)	1092	
Crystal size	0.41 x 0.15 x 0.05 mm <sup>3</sup>	
Theta range for data collection	1.72 to 25.54°.	
Index ranges	-14 ≤ h ≤ 14, 0 ≤ k ≤ 13, 0 ≤ l ≤ 17	
Reflections collected	65700	
Independent reflections	3674 [R(int) = 0.126]	
Completeness to theta = 25.00°	100.0 %	
Absorption correction	Semi-empirical from equivalents	
Max. and min. transmission	0.9319 and 0.6058	
Refinement method	Full-matrix least-squares on F <sup>2</sup>	
Data / restraints / parameters	3674 / 0 / 225	
Goodness-of-fit on F <sup>2</sup>	1.191	
Final R indices [I > 2σ(I)]	R1 = 0.0791, wR2 = 0.2156	
R indices (all data)	R1 = 0.0959, wR2 = 0.2222	
Largest diff. peak and hole	2.982 and -2.661 e.Å <sup>-3</sup>	

**Table S18.** Bond length [Å] for lm24010

Pd(1)-N(2)	2.002(8)	C(7)-H(7B)	0.9900
Pd(1)-N(1)	2.029(8)	C(8)-C(9)	1.362(15)
Pd(1)-Cl(1)	2.303(3)	C(9)-C(10)	1.393(15)
Pd(1)-N(3)	2.310(9)	C(9)-H(9)	0.9500
Pd(1)-N(4)	2.311(9)	C(10)-C(11)	1.375(15)
Pd(1)-Cl(2)	2.322(3)	C(10)-H(10)	0.9500
Cl(3)-O(4)	1.430(8)	C(11)-C(12)	1.376(14)
Cl(3)-O(2)	1.440(8)	C(11)-H(11)	0.9500
Cl(3)-O(3)	1.441(8)	C(12)-C(13)	1.493(14)
Cl(3)-O(1)	1.451(8)	C(13)-H(13A)	0.9900
N(1)-C(5)	1.329(13)	C(13)-H(13B)	0.9900
N(1)-C(1)	1.365(14)	C(14)-H(14A)	0.9900
N(2)-C(8)	1.335(13)	C(14)-H(14B)	0.9900
N(2)-C(12)	1.365(13)	C(15)-H(15A)	0.9800
N(3)-C(7)	1.473(14)	C(15)-H(15B)	0.9800
N(3)-C(6)	1.474(14)	C(15)-H(15C)	0.9800
N(3)-C(15)	1.475(14)	C(16)-H(16A)	0.9800
N(4)-C(16)	1.464(14)	C(16)-H(16B)	0.9800
N(4)-C(13)	1.471(14)	C(16)-H(16C)	0.9800
N(4)-C(14)	1.496(13)		
C(1)-C(2)	1.373(15)		
C(1)-C(14)	1.481(14)		
C(2)-C(3)	1.382(16)		
C(2)-H(2)	0.9500		
C(3)-C(4)	1.391(17)		
C(3)-H(3)	0.9500		
C(4)-C(5)	1.378(15)		
C(4)-H(4)	0.9500		
C(5)-C(6)	1.518(15)		
C(6)-H(6A)	0.9900		
C(6)-H(6B)	0.9900		
C(7)-C(8)	1.505(15)		
C(7)-H(7A)	0.9900		

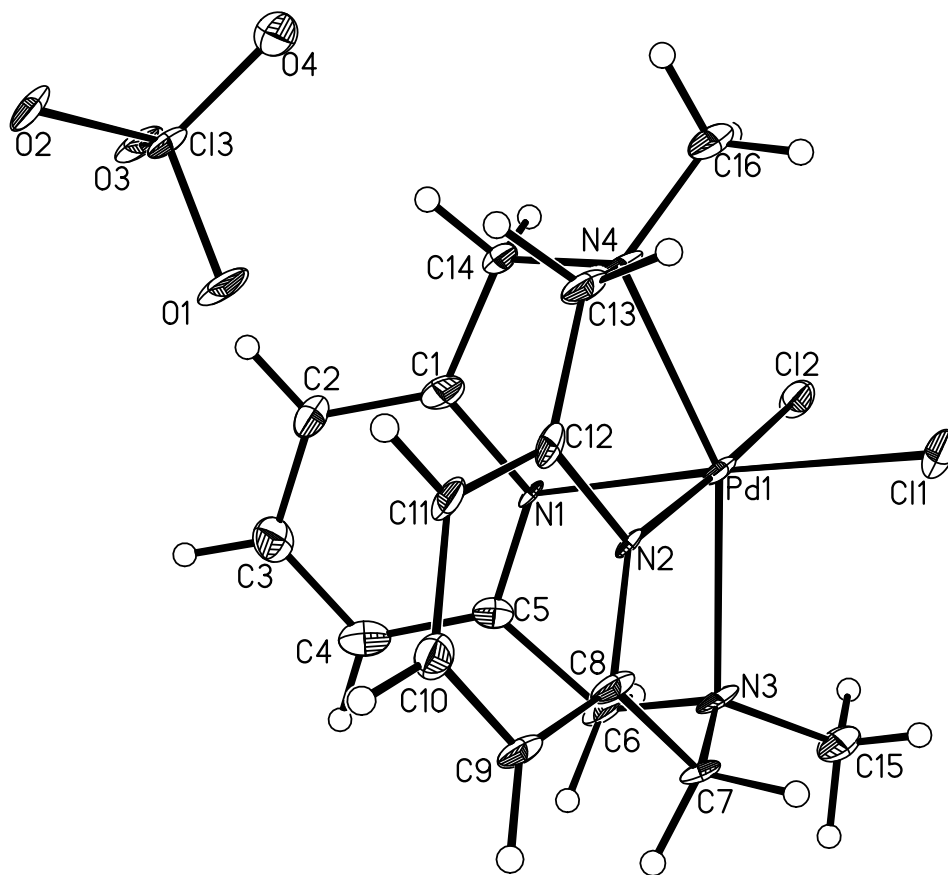


**Figure S40.** Projection view of  $[2^+]\text{ClO}_4$  with 50% thermal ellipsoids.

### X-ray structure determination of [(<sup>Me</sup>N<sup>4OMe</sup>)Pd<sup>III</sup>MeCl]ClO<sub>4</sub>, [4<sup>+</sup>]ClO<sub>4</sub>

**Table S19.** Crystal data and structure refinement for lm17312.

Identification code	117312/lt/FT-081312	
Empirical formula	C <sub>19</sub> H <sub>27</sub> Cl <sub>2</sub> N <sub>4</sub> O <sub>6</sub> Pd	
Formula weight	584.75	
Temperature	100(2) K	
Wavelength	0.71073 Å	
Crystal system	Monoclinic	
Space group	P2 <sub>1</sub> /n	
Unit cell dimensions	a = 12.1464(6) Å	α = 90°.
	b = 15.0961(7) Å	β = 114.078(2)°.
	c = 13.8150(7) Å	γ = 90°.
Volume	2312.8(2) Å <sup>3</sup>	
Z	4	
Density (calculated)	1.679 Mg/m <sup>3</sup>	
Absorption coefficient	1.077 mm <sup>-1</sup>	
F(000)	1188	
Crystal size	0.35 x 0.29 x 0.19 mm <sup>3</sup>	
Theta range for data collection	1.89 to 27.54°.	
Index ranges	-15 ≤ h ≤ 15, -19 ≤ k ≤ 19, -17 ≤ l ≤ 17	
Reflections collected	31754	
Independent reflections	5326 [R(int) = 0.0374]	
Completeness to theta = 27.54°	99.7 %	
Absorption correction	Semi-empirical from equivalents	
Max. and min. transmission	0.8240 and 0.7070	
Refinement method	Full-matrix least-squares on F <sup>2</sup>	
Data / restraints / parameters	5326 / 54 / 307	
Goodness-of-fit on F <sup>2</sup>	1.191	
Final R indices [I > 2σ(I)]	R1 = 0.0420, wR2 = 0.0872	
R indices (all data)	R1 = 0.0522, wR2 = 0.0913	
Largest diff. peak and hole	0.605 and -0.785 e.Å <sup>-3</sup>	

**Table S20.** Bond lengths [Å] and angles [°] for lm17312.

Pd(1)-C(1)	2.040(4)	C(2)-C(15)	1.511(5)
Pd(1)-N(1)	2.055(3)	C(3)-C(4)	1.391(5)
Pd(1)-N(2)	2.130(3)	C(3)-H(3)	0.9500
Pd(1)-N(3)	2.297(3)	C(4)-C(5)	1.387(5)
Pd(1)-Cl(1)	2.3298(11)	C(5)-C(6)	1.383(5)
Pd(1)-N(4)	2.340(3)	C(5)-H(5)	0.9500
O(1)-C(4)	1.351(4)	C(6)-C(7)	1.502(5)
O(1)-C(18)	1.440(5)	C(7)-H(7A)	0.9900
O(2)-C(11)	1.345(5)	C(7)-H(7B)	0.9900
O(2)-C(19)	1.436(5)	C(8)-C(9)	1.507(6)
Cl(2)-O(6)	1.399(4)	C(8)-H(8A)	0.9900
Cl(2)-O(3')	1.405(13)	C(8)-H(8B)	0.9900
Cl(2)-O(4)	1.426(4)	C(9)-C(10)	1.371(6)
Cl(2)-O(5')	1.428(11)	C(10)-C(11)	1.400(5)
Cl(2)-O(4')	1.436(13)	C(10)-H(10)	0.9500
Cl(2)-O(3)	1.443(4)	C(11)-C(12)	1.386(5)
Cl(2)-O(5)	1.473(4)	C(12)-C(13)	1.383(5)
Cl(2)-O(6')	1.529(12)	C(12)-H(12)	0.9500
N(1)-C(2)	1.334(5)	C(13)-C(14)	1.502(5)
N(1)-C(6)	1.339(5)	C(14)-H(14A)	0.9900
N(2)-C(13)	1.336(5)	C(14)-H(14B)	0.9900
N(2)-C(9)	1.343(5)	C(15)-H(15A)	0.9900
N(3)-C(8)	1.477(5)	C(15)-H(15B)	0.9900
N(3)-C(16)	1.482(5)	C(16)-H(16A)	0.9800
N(3)-C(7)	1.483(5)	C(16)-H(16B)	0.9800
N(4)-C(15)	1.475(5)	C(16)-H(16C)	0.9800
N(4)-C(17)	1.475(5)	C(17)-H(17A)	0.9800
N(4)-C(14)	1.483(5)	C(17)-H(17B)	0.9800
C(1)-H(1A)	0.9800	C(17)-H(17C)	0.9800
C(1)-H(1B)	0.9800	C(18)-H(18A)	0.9800
C(1)-H(1C)	0.9800	C(18)-H(18B)	0.9800
C(2)-C(3)	1.373(5)	C(18)-H(18C)	0.9800

C(19)-H(19A)  
C(19)-H(19B)

0.9800  
0.9800

C(19)-H(19C)

0.9800

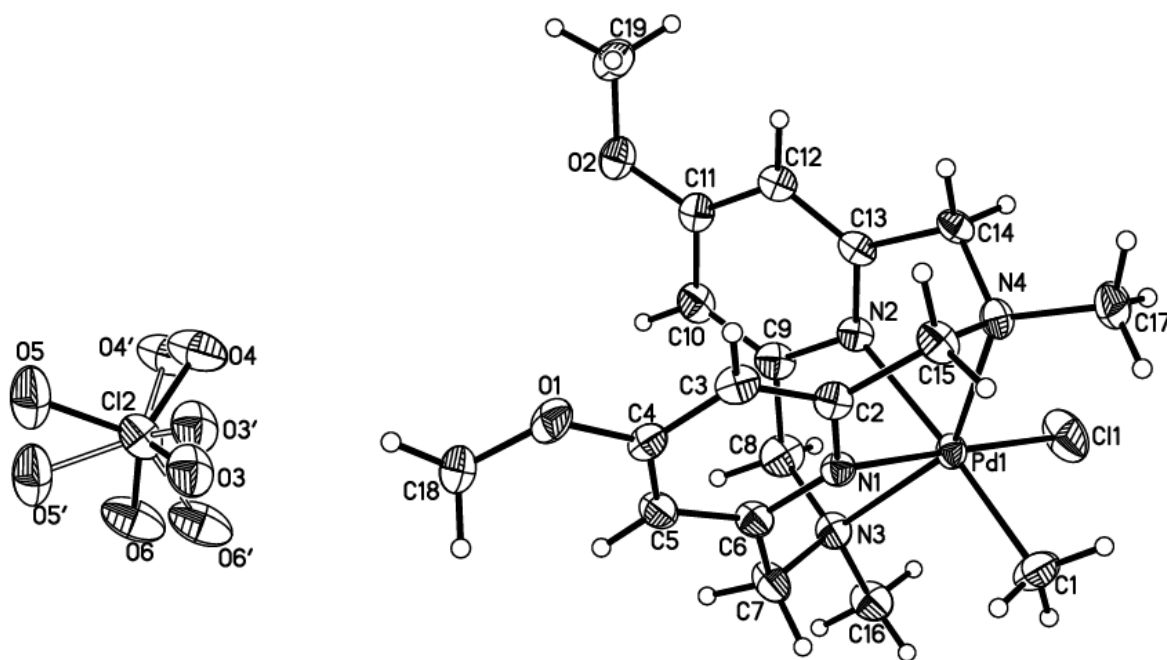


**Figure S41.** Projection view of  $[4^+]\text{C10}_4$  with 50% thermal ellipsoids.

## IX. References

1. G. K. Anderson, M. Lin, A. Sen, E. Gretz, in *Inorg. Synth.*, John Wiley & Sons, Inc., 2007, pp. 60.
2. R. E. Rulke, J. M. Ernsting, A. L. Spek, C. J. Elsevier, P. W. N. M. v. Leeuwen, K. Vrieze, *Inorg. Chem.*, 1993, **32**, 5769.
3. F. Tang, F. Qu, J. R. Khusnutdinova, N. P. Rath, L. M. Mirica, *Dalton Trans.*, 2012, **41**, 14046.
4. D. F. Evans, *J. Chem. Soc.*, 1959, 2003.
5. G. A. Bain, J. F. Berry, *J. Chem. Educ.*, 2008, **85**, 532.
6. A.-L. Gassner, C. I. Duhot, J.-C. G. Bünzli, A.-S. Chauvin, *Inorg. Chem.*, 2008, **47**, 7802.
7. A. D. Becke, *J. Chem. Phys.*, 1993, **98**, 1372.
8. C. T. Lee, W. T. Yang, R. G. Parr, *Phys. Rev. B- Cond. Matter*, 1988, **37**, 785.
9. W. J. Stevens, H. Basch, M. Krauss, *J. Chem. Phys.*, 1984, **81**, 6026.
10. W. J. Stevens, M. Krauss, H. Basch, P. G. Jasien, *Can. J. Chem.*, 1992, **70**, 612.
11. N. A. Foley, M. Lail, J. P. Lee, T. B. Gunnoe, T. R. Cundari, J. L. Petersen, *J. Am. Chem. Soc.*, 2007, **129**, 6765.
12. A. S. Veige, L. M. Slaughter, P. T. Wolczanski, N. Matsunaga, S. A. Decker, T. R. Cundari, *J. Am. Chem. Soc.*, 2001, **123**, 6419.
13. L. Skripnikov, *Chemissian, version 1.771, 2010*, [www.chemissian.com](http://www.chemissian.com), accessed June 2016.
14. N. M. O'Boyle, A. L. Tenderholt, K. M. Langner, *J. Comput. Chem.*, 2008, **29**, 839.